Molecular Therapy
Nucleic Acids
Original Article

Extracellular vesicles enriched with an endothelial cell pro-survival microRNA affects skin tissue regeneration

Hugo Fernandes,[1,2] Alessandra Zonnari,[1] Ricardo Abreu,[1,3,4,5] Sezin Aday,[1] Marta Barão,[1] Inês Albino,[1] Miguel Lino,[1] Ana Branco,[1] Cátia Seabra,[1] Tânia Barata,[1] Ermelindo C. Leal,[1,6] José Guilherme Tralhão,[2,7] Lino Gonçalves,[2] Alwin de Jong,[8,9] Hendrika A.B. Peters,[8,9] Margreet R. de Vries,[8,9] Paula da Costa Martins,[4,5] Paul H.A. Quax,[8,9] and Lino Ferreira[1,2]

[1]CNC-Center for Neuroscience and Cell Biology, CIBB-Centre for Innovative Biomedicine and Biotechnology, University of Coimbra, UC, Biotech Parque Tecnológico de Cantanhede, 3060-197 Coimbra, Portugal; [2]Faculty of Medicine, University Coimbra, 3000-548 Coimbra, Portugal; [3]CARIM School for Cardiovascular Diseases, Faculty of Health, Medicine and Life Sciences, Maastricht University, 6200 MD Maastricht, the Netherlands; [4]Department of Molecular Genetics, Faculty of Sciences and Engineering, Maastricht University, 6200 MD Maastricht, the Netherlands; [5]PhD Programme in Experimental Biology and Biomedicine, Institute for Interdisciplinary Research (IIIUC), University of Coimbra, Casa Costa Alemão, 3030-789 Coimbra, Portugal; [6]Institute of Interdisciplinary Research, University of Coimbra, 3030-789 Coimbra, Portugal; [7]Department of Surgery, Centro Hospitalar e Universitário de Coimbra (CHUC), University Hospital, Faculty of Medicine, 3000-075 Coimbra, Portugal; [8]Department of Surgery, Leiden University Medical Center, 2300 RC Leiden, the Netherlands; [9]Einthoven Laboratory for Experimental Vascular Medicine, Leiden University Medical Center, 2300 RC Leiden, the Netherlands

Endothelial cell (EC) activity is essential for tissue regeneration in several (patho)physiological contexts. However, our capacity to deliver *in vivo* biomolecules capable of controlling EC fate is relatively limited. Here, we screened a library of microRNA (miR) mimics and identified 25 miRs capable of enhancing the survival of ECs exposed to ischemia-mimicking conditions. *In vitro*, we showed that miR-425-5p, one of the hits, was able to enhance EC survival and migration. *In vivo*, using a mouse Matrigel plug assay, we showed that ECs transfected with miR-425-5p displayed enhanced survival compared with scramble-transfected ECs. Mechanistically, we showed that miR-425-5p modulated the PTEN/PI3K/AKT pathway and inhibition of miR-425-5p target genes (*DACH1*, *PTEN*, *RGS5*, and *VASH1*) phenocopied the pro-survival. For the *in vivo* delivery of miR-425-5p, we modulated small extracellular vesicles (sEVs) with miR-425-5p and showed, *in vitro*, that miR-425-5p-modulated sEVs were (1) capable of enhancing the survival of ECs exposed to ischemia-mimic conditions, and (2) efficiently internalized by skin cells. Finally, using a streptozotocin-induced diabetic wound healing mouse model, we showed that, compared with miR-scrambled-modulated sEVs, topical administration of miR-425-5p-modulated sEVs significantly enhanced wound healing, a process mediated by enhanced vascularization and skin re-epithelialization.

INTRODUCTION

A complex interplay between cellular and molecular players, acting in a spatial-temporal controlled manner, is critical for tissue regeneration.[1] Angiogenesis, the physiological process through which new blood vessels form from pre-existing vessels, is an important mechanism in wound regeneration. Unfortunately, aging and metabolic diseases negatively affect angiogenesis, ultimately compromising wound regeneration. Endothelial cells (ECs) are the main players in angiogenesis and, thus, impairment of EC function and/or number in wounds leads to a concomitant reduction in neovascularization. Hence, pro-angiogenic and/or pro-survival signals specifically directed toward ECs are crucial to enhance wound vascularization.

Given the multifactorial nature of the neovascularization process, microRNAs (miRs) emerged as a novel therapeutic target to enhance vascularization.[2] miRs are a class of small, single-stranded, non-coding RNA (2025 nucleotides) that repress the expression of target messenger RNA (mRNA) by base pairing, with perfect or imperfect complementarity sequences, at the 3 UTR. The sequence of two to eight nucleotides at the 5 end of the miR, called the seed sequence, is normally sufficient to direct it to its target, where it will inhibit translation or promote its degradation. Since as few as seven complementary nucleotides are needed to bind to the target, one miR can modulate thousands of different targets, and this multi-targeting

Received 19 November 2021; accepted 18 March 2022;
https://doi.org/10.1016/j.omtn.2022.03.018.

Correspondence: Lino Ferreira, CNC-Center for Neuroscience and Cell Biology, CIBB-Centre for Innovative Biomedicine and Biotechnology, University of Coimbra, UC, Biotech Parque Tecnológico de Cantanhede, 3060-197 Coimbra, Portugal.
E-mail: lino@uc-biotech.pt
Correspondence: Hugo Fernandes, CNC-Center for Neuroscience and Cell Biology, CIBB-Centre for Innovative Biomedicine and Biotechnology, University of Coimbra, UC, Biotech Parque Tecnológico de Cantanhede, 3060-197 Coimbra, Portugal.
E-mail: hugo.fernandes@uc.pt

This is an open access article under the CC BY-NC-ND license (http://creativecommons.org/licenses/by-nc-nd/4.0/).

potential can be harnessed for therapeutic interventions where simultaneous modulation is needed.[3,4]

Several miRs have been reported to control EC activity and/or function. For example, we have shown that inhibition of 14q32 miRs miR-329, miR-487b, miR-494, and miR-495 increased neovascularization and blood flow recovery after ischemia.[5] Moreover, it has been shown that downregulation of miR-200b, specifically in ECs, accelerated wound angiogenesis in a process partially mediated by modulation of vascular endothelial growth factor (VEGF) signaling.[6] In addition, the inhibition of miR-92a, a miR belonging to the miR-17–92 cluster, highly expressed in EC and previously reported as critical for angiogenesis, enhanced the regeneration of wounds in diabetic mice by improving proliferation and angiogenesis.[7,8] In diabetic mice (db/db mice), topical administration of miR-27b enhanced wound healing by, at least partially, increasing wound vascularization.[9] Moreover, the inhibition of miR-26a, highly expressed in wounds of db/db mice, led to a significant increase in wound vascularization (>80% compared with control) and ultimately accelerated wound closure.[10] Furthermore, in the same animal model, it was shown that wounds treated with a miR-210 inhibitor closed 4 days earlier than untreated wounds, partially by increasing proliferation and vascularization.[11] Unfortunately, our knowledge about miRs able to interfere with EC survival is limited,[12,13] and this is important in the context of skin wound healing since ECs are critical for neovascularization after the inflammatory phase.[1]

A separate challenge regarding the use of miRs for skin wound healing relates to their delivery. Indeed, *in vivo* miR delivery remains challenging owing to (1) fast clearance from circulation, (2) poor cellular uptake, and (3) limited capacity to escape the endo-lysosomal compartment and reach the cytoplasm where their processing machinery and target(s) are present. Encapsulating and/or conjugating miRs in nanocarriers is a strategy commonly used to protect miRs from degradation, increase their half-life and, by tailoring the nanocarrier, endow the user with countless possibilities to control the delivery in a spatial-temporal manner.[14] Small extracellular vesicles (sEVs), vesicles with a diameter ~100 nm and secreted by virtually every cell within the body, are key mediators of intercellular communication.[15,16] The innate capacity of sEVs to transfer biomolecular information between cells in a paracrine and/or endocrine-like manner has been exploited as a standalone therapy as well as for drug delivery applications. For example, atorvastatin-treated mesenchymal stromal cells secreted sEVs containing pro-angiogenic factors, namely miR-221-3p, that activated AKT/eNOS pathway and ultimately enhanced wound closure in diabetic rats by increasing angiogenesis.[17] In addition, the electroporation of sEVs with miR-21-5p has been reported to accelerate diabetic wound healing by increasing angiogenesis and vessel maturation.[18] However, the best strategy to load a miR of interest in sEVs is still disputable. Recently, we compared the efficiency of different methodologies to load a miR of interest into sEVs isolated from several sources and showed that, in the conditions tested, a chemical strategy based on the transfection agent Exo-Fect was superior to other methods, including the transfection of sEV-secreting cells or the post-isolation modulation of sEVs by methods such as electroporation, heat-shock, detergent-based permeabilization or conjugation of miRs with cholesterol.[19]

In the current study, we identified miRs capable of enhancing the survival of ECs cultured in ischemia-mimicking conditions and developed an efficient strategy to load these miRs in sEVs for their *in vivo* delivery. Initially, we screened a library of 2,080 human miR mimics and identified 15 miRs (eight previously known and seven not previously identified as pro-survival miRs) that significantly increased the survival of ECs in ischemia-mimicking conditions. Subsequently, we selected two miRs (miR-425-5p and miR-5692c) to investigate their role in EC migration and angiogenesis and studied their mechanism of action. Next, we investigated the role of one of the miRs (miR-425-5p; conserved between species) in the survival of ECs transplanted *in vivo*. Finally, we developed a platform for the *in vivo* delivery of one of the miRs using sEVs and evaluated their effect in a diabetic wound healing animal model. Our results indicate that the topical delivery of an EC pro-survival miR using sEVs significantly accelerated wound closure through enhanced vascularization and re-epithelialization of the wound area.

RESULTS

Identification of pro-survival miRs using high-content screening assay

For the identification of pro-survival miRs, we used human $CD34^+$ cell-derived outgrowth endothelial progenitor cells.[20] These cells directly participate in tubulogenesis[21] and their neovascularization potential has been demonstrated in pre-clinical tests using different animal models of hindlimb ischemia and diabetic chronic wounds, among others.[22–26] A library containing 2,080 human miR mimics was screened to identify miRs capable of enhancing the survival of $CD34^+$-derived ECs in ischemic conditions (EBM-2 and 0.1% O_2) (Figure 1A). Twenty-five miRs were identified as pro-survival miRs based on the criteria described (see section "materials and methods") (Figure 1B and Table S2). To validate the results of the primary screening, we performed a secondary screening using the same experimental conditions but now with three technical replicates per miR. Based on a statistically significant difference between the selected miR and Lipofectamine-treated cells, we were able to confirm the pro-survival effect of 15 miRs: miR-26a-5p, miR-642a-3p, miR-425-5p, miR-26b-5p, miR-199-3p, miR-380-3p, miR-5692c, miR-4695-5p, miR-3147, miR-3164, miR-32-3p, miR-4713-5p, miR-638, miR-4253, and miR-3171 (Figure 1C and Table S3).

Effect of miR-425-5p and miR-5692c on EC functionality

From the list of confirmed pro-survival miRs, we selected two miRs for further analysis: miR-425-5p and miR-5692c. These miRs have not been described as EC pro-survival miRs. For both miRs, we first selected the concentration necessary to elicit a pro-survival effect using three EC models: $CD34^+$-derived ECs, human umbilical vein ECs (HUVECs), and human umbilical arterial endothelial cells (HUAECs). Our results showed that, except in the case of miR-425-5p in HUAECs, for both miRs, a concentration of 25 nM led to a

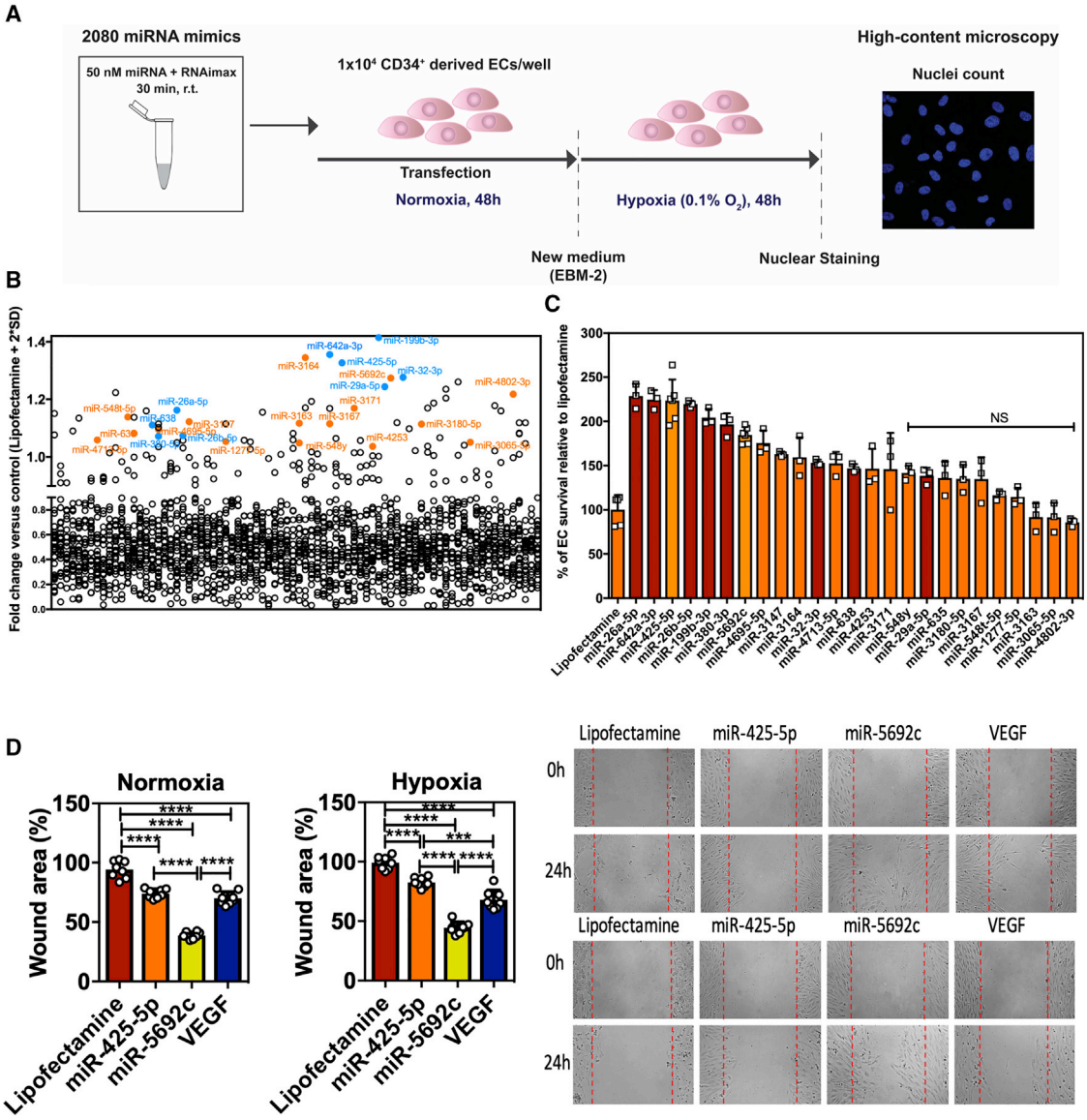

Figure 1. HCS assay

(A) Schematic overview of the HCS assay implemented to identify EC pro-survival miRs. CD34$^+$-derived ECs, cultured in EGM-2 medium, were transfected for 48 h with a library of 2,080 human miR mimics using Lipofectamine RNAiMAX. Subsequently, the transfection medium was replaced by EBM-2 medium and the cells were transferred to a hypoxia chamber (0.1% O) and cultured for further 48 h, upon which nuclear staining was performed and images acquired using a high-content microscope. Per plate, Lipofectamine-treated cells were used as a control. (B) Primary screening results. The screening was repeated twice using two different donors. Data points in the graph represent the mean of both replicates relative to Lipofectamine. Blue dots denote miRs previously associated with survival, whereas orange dots denote miRs not previously associated with survival. (C) Secondary screening results. Cell survival was evaluated by counting the number of cells that survived in ischemic conditions for 48 h. The results were normalized by Lipofectamine-treated cell condition. Bordeaux bars represent miRs previously associated with enhanced survival, whereas orange bars represent miRs not previously described as pro-survival miRs. Data points in the graph represent the mean ± SD (n = 3 technical replicates per condition). Statistical difference was calculated by a one-way ANOVA test followed by Tukey's multiple comparison test. *$p < 0.05$. (D) Effect of miR-425-5p and miR-5692c in the migration of CD34$^+$-derived ECs cultured under normoxia or hypoxia (0.1% O_2) conditions (see section "materials and methods"). Medium containing $VEGF_{165}$ was used as positive control. Per experimental condition, the wound area was determined using the following formula: (wound size after 24 h/wound size at 0 h) × 100. Statistical analyses were performed by one-way ANOVA followed by a Tukey's multiple comparison test. ***$p < 0.001$ and ****$p < 0.0001$. Results are presented as mean ± SD (n = 3 biological replicates, each biological replicate containing three technical replicates).

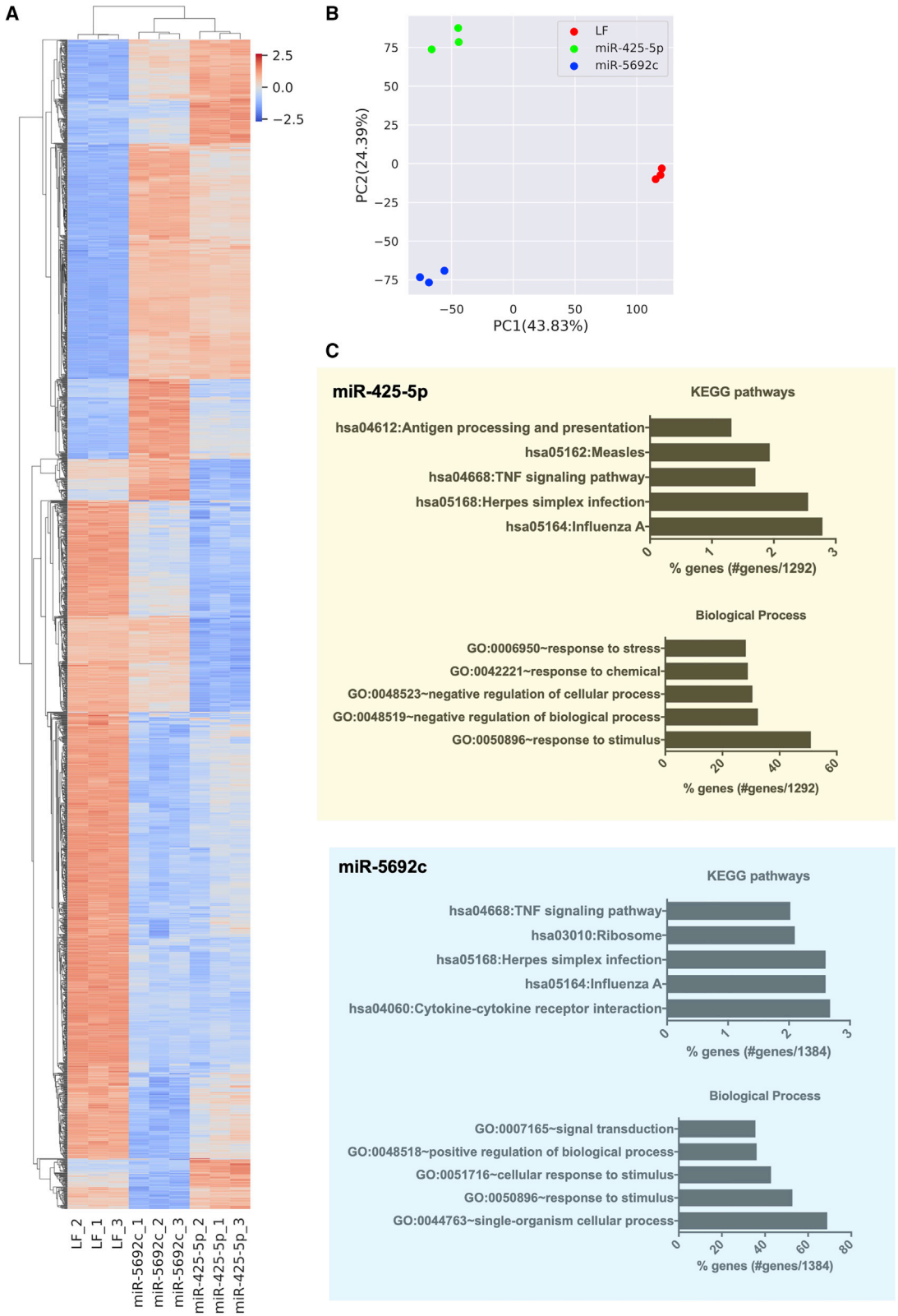

(legend on next page)

statistically significant increase in EC survival upon exposure to ischemic conditions (Figure S1). Next, we confirmed that, upon transfection of $CD34^+$-derived ECs with miR-425-5p or miR-5692c, the endothelial phenotype was maintained. Western blot analysis and immunocytochemistry (ICC) showed that, upon transfection, the expression of VE-cadherin was maintained and, as expected, localized at the cell membrane (Figure S2). Finally, we performed a migration and angiogenesis assay on $CD34^+$-derived ECs, HUVECs, and HUAECs transfected with 25 nM miR-425-5p or miR-5692c. Our results showed that miR-425-5p improved wound closure, in a statistically significant manner, solely on $CD34^+$-derived ECs, independent of the culture conditions (hypoxia or normoxia). In contrast, miR-5692c improved wound closure, in a statistically significant manner, in all conditions regardless of the EC phenotype and the culture conditions (hypoxia or normoxia) (Figure S3). In contrast with the results obtained for the migration, our results showed that neither miR-425-5p nor miR-5692c led to a statistically significant increase in the number of tube-like structures, i.e., a marker of angiogenesis, compared with Lipofectamine-treated cells. In fact, regardless of the culture conditions, HUAECs transfected with miR-5692c showed a statistically significant reduction in the number of tube-like structures compared with Lipofectamine-treated cells (Figure S4). Overall, our results indicate that both miR-425-5p and miR-5692c significantly increase EC survival in ischemic conditions and enhanced EC migration, the latter being dependent on the miR, culture conditions and EC phenotype. Compared with control, both miR-425-5p and miR-5692c had no positive effect in angiogenesis as evaluated by a Matrigel tube formation assay.

miR-425-5p and miR-5692c mechanism of action

To unravel the pro-survival mechanism of action of miR-425-5p and miR-5692c, we performed RNA sequencing (RNA-seq) and *in silico* target prediction analysis. First, hierarchical clustering and principal component analysis (PCA) was performed on the list of differentially expressed genes (DEGs) (miR-425-5p versus Lipofectamine, 1,292 DEG, 528 upregulated and 764 downregulated; miR-5692c, 1,384 DEG, 579 upregulated and 805 downregulated; Tables S4 and S5, respectively) and showed that, despite eliciting the same biological response (enhancing the survival of ECs), the transcriptome of miR-425-5p- and miR-5692c-transfected ECs was significantly different from the control as well as between both miRs (Figures 2A, 2B, and S5). Next, we used Gene Ontology (GO) enrichment analysis to identify the main biological processes and signaling pathways modulated by both miRs. In the case of miR-425-5p, the top 5 signaling pathways (influenza A, herpes simplex infection, tumor necrosis factor [TNF] signaling pathway, measles, and antigen processing and presentation) and biological processes (type I interferon signaling pathway, defense response to virus, interferon-gamma-mediated signaling pathway, negative regulation of viral genome replication, and response to virus) suggested that an inflammatory program has been activated upon transfection (Figure 2C; Table S6). Interestingly, in the case of miR-5692c, the top five biological processes were similar to miR-425-5p, as were three of the top five pathways (influenza A, herpes simplex infection, and TNF signaling pathway), again suggesting an inflammatory signature elicited by the transfection of cells with miR-5692c (Figure 2C; Table S7).

Next, we set out to identify the putative targets of miR-425-5p and miR-5692c. To select the genes of interest for further validation, we used three separate strategies (Figure 3A). In strategy 1, we intersected the list of differentially expressed downregulated genes obtained by RNA-seq with the list of genes retrieved from miRWalk (136 genes for miR-425-5p and 43 genes for miR-5692c; Tables S8 and S9, respectively) and selected a list of seven genes that were common to both miRs (Table S10), which, upon literature mining for their involvement on cell survival, was reduced to four genes used for further validation: *RGS5*, *AIF1L*, *BCL2L11*, and *CBX5*. For strategy 2 and 3, we only focused on miR-425-5p since it was the only miR conserved in different species. In strategy 2, from the list of downregulated genes obtained in strategy 1 (after merging the downregulated genes from RNA-seq with the miRWalk list, a total of 136 downregulated genes for miR-425-5p), we selected the genes with a $\log_2$ fold change (FC) < 2 (17 genes in total; Table S8) and, upon literature mining, we selected four out of 17 genes for further validation: *DACH1*, *CMTM3*, *VASH1*, and *CADM4*. Finally, in strategy 3, we retrieved from the literature a list of genes validated as direct targets of miR-425-5p and described as having a role in cell survival, regardless of the cell type (14 genes in total; Table S11). For these 14 genes, we analyzed the average expression (fragments per kilobase of transcript per million mapped reads [FPKM]) in our RNA-seq dataset and, after excluding genes with an expression level higher in miR-425-5p than the control and genes with an FPKM <10 in the control group, we selected three genes for further validation: *PDCD10*, *ADAM9*, and *PTEN*. Thus, the final list for validation by RT-PCR comprised 11 genes: *RGS5*, *AIF1L*, *BCL2L11*, *CBX5*, *DACH1*, *CMTM3*, *VASH1*, *CADM4*, *PDCD10*, *ADAM9*, and *PTEN*. Our validation by qPCR analysis showed a statistically significant difference between miR-425-5p-transfected ECs and the control solely for *CADM4*, *CBX5*, *CMTM3*, *DACH1*, *PTEN*, *RGS5*, and *VASH1* (Figure 3B) but no differences for *ADAM9*, *AIF1L*, *BCL2L11*, and *PDCD10* (Figure S6A).

To functionally validate the pro-survival role of these genes, we knocked down each of them using short interfering RNA (siRNA) and analyzed their effect on cell survival using the same experimental conditions described for the primary screening. Our results showed that inhibition of *DACH1, PTEN, RGS5,* and *VASH1* enhanced the

Figure 2. RNA-seq analyses

$CD34^+$-derived ECs were transfected for 48 h with 25 nM miR-425-5p or miR-5692c using Lipofectamine RNAiMAX. After 48 h cells were lysed, total RNA isolated and a library was prepared to perform RNA-seq. Hierarchical clustering (A), PCA analysis (B) and gene enrichment analysis (C) were performed using the list of DEGs (for miR-425-5p, a total of 1,292 genes was used, 528 upregulated and 764 downregulated, whereas for miR-5692c a total of 1,384 genes was used, 579 upregulated and 805 downregulated).

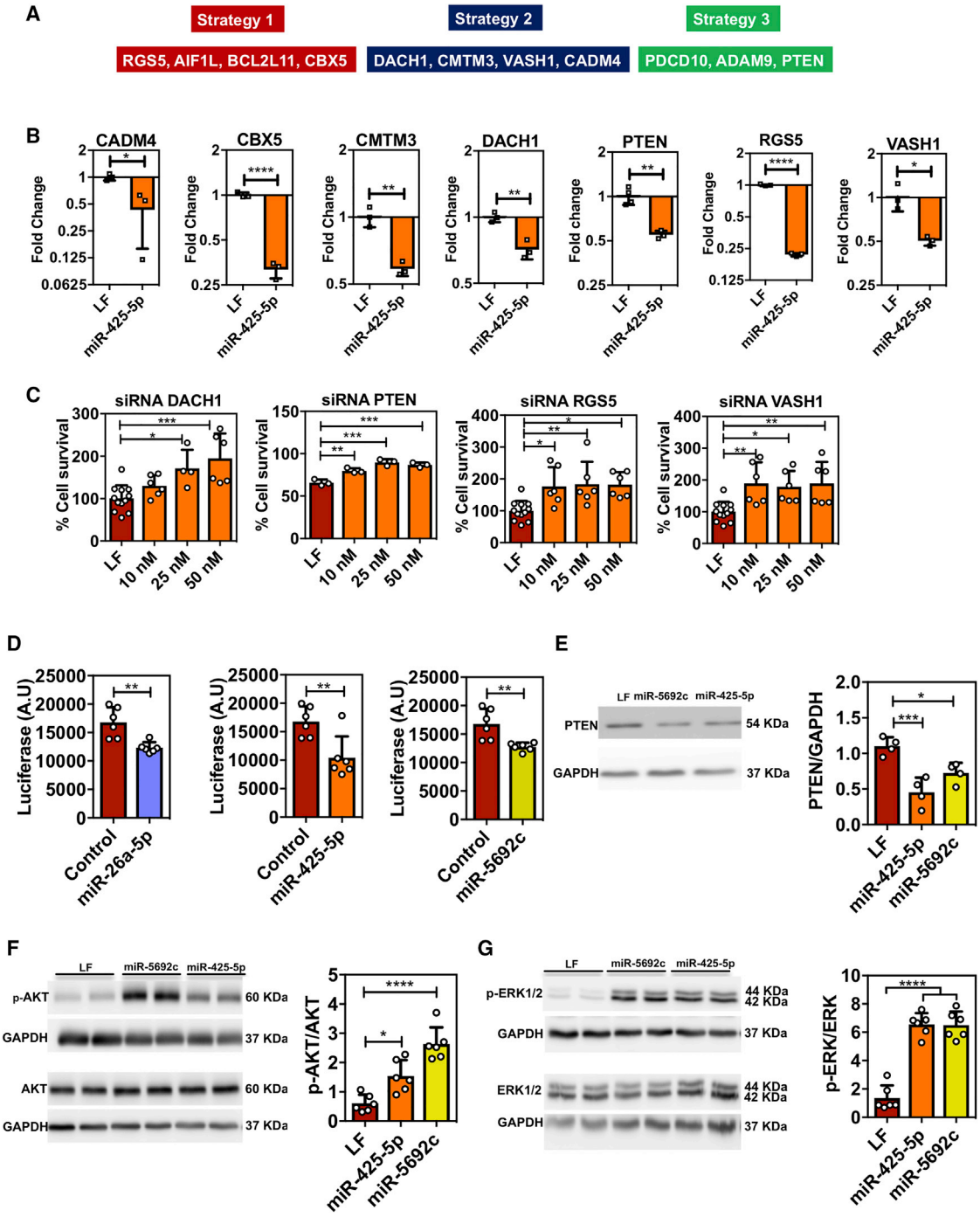

Figure 3. Mechanism of action of miR-425-5p and miR-5692c

(A) Overview of the three strategies used to identify 11 putative targets of miR-425-5p and miR-5692c. (B) Validation of miR-425-5p putative target genes. qRT-PCR analyses confirmed the downregulation of seven of the 11 putative target genes upon transfection of $CD34^+$-derived ECs for 48 h with 25 nM miR-425-5p. Results are mean ± SD (n = 1 biological replicate, each biological replicate containing three independent technical replicates). Statistical analysis was performed by an unpaired t test. LF, Lipofectamine. (C) Demonstration of the importance of the molecular targets for the pro-survival mechanism of miR-425-5p. $CD34^+$-derived ECs were transfected, for 48 h, with different concentrations of siRNAs targeting the putative targets of miR-425-5p. Subsequently, the transfection medium was replaced by EBM-2 medium and the cells were transferred to a hypoxia chamber (0.1% O_2) and cultured for further 48 h, upon which nuclear staining was performed and images acquired using a high-content microscope. Lipofectamine-treated cells were used as a control. Statistical analyses were performed by one-way ANOVA followed by a Tukey's multiple comparison test. Results are

(legend continued on next page)

survival of $CD34^+$-derived ECs in at least two of the concentrations tested, whereas inhibition of *CADM4* and *CBX5* was less robust (the effect was only observed for one of the concentrations tested, which can be, at least partially, attributed to the limited knockdown efficiency) (Figures 3C, S6B, and S6C). Altogether, our transcriptomic results showed that miR-425-5p and miR-5692c induced an inflammatory program in ECs and the pro-survival effect was mediated by the regulation of *PTEN*, *DACH1*, *RGS5*, and *VASH1*.

PTEN is a direct target of miR-425-5p and miR-5692c

Given the well-described role of PTEN in cell survival,[27] we confirmed, as predicted, that miR-425-5p and miR-5692c directly interact with the 3′ UTR from *PTEN* mRNA (Figure S7) and that PTEN protein levels were downregulated upon transfection with both miRs. To demonstrate that miR-425-5p and miR-5692c interacted with the 3′ UTR of *PTEN* mRNA, we used a luciferase-based reporter assay consisting of a constitutive promoter driving the expression of luciferase and a fragment of the 3′ UTR of *PTEN* mRNA cloned downstream of the luciferase gene. Our results showed a statistically significant inhibition of luciferase expression upon transfection with miR-26a-5p, a miR known to interact with the 3′ UTR of *PTEN* mRNA. Moreover, a similar inhibition was observed upon transfection of miR-425-5p and miR-5692c, confirming a direct interaction of both miRs with the 3′ UTR of *PTEN* mRNA (Figure 3D). Next, we evaluated if the direct interaction of miR-425-5p and miR-5692c with the 3′ UTR *PTEN* mRNA led to a reduction in PTEN protein levels. Western blot analysis confirmed the downregulation of PTEN protein upon transfection of $CD34^+$-derived ECs with both miRs (Figure 3E). Our results further showed that transfection of $CD34^+$-derived ECs with miR-425-5p and miR-5692c significantly increased AKT phosphorylation compared with Lipofectamine-treated cells (Figure 3F). Moreover, upon transfection of $CD34^+$-derived ECs with miR-425-5p and miR-5692c, there was a significant increase in the phosphorylation of ERK1/2 (Figure 3G). Based on these results, we concluded that inhibition of *PTEN* by miR-425-5p or miR-5692c led to an increase in the survival of $CD34^+$-derived ECs in ischemic conditions, at least partially, by increasing the phosphorylation of AKT and ERK1/2, both well-recognized pro-survival pathways.

miR-425-5p enhanced the survival of ECs in an *in vivo* Matrigel plug assay

In contrast to miR-5692c, miR-425-5p is conserved throughout different species and was thus selected for further *in vivo* studies. To test whether the transfection of ECs with miR-425-5p enhanced their survival *in vivo*, we used the *in vivo* Matrigel plug assay in mice (Figure 4A). Firstly, we showed that 24 h after transfection of ECs with 25 nM miR-425-5p there was a statistically significant upregulation (>30,000 FC) in the expression of miR-425-5p compared with miR-scramble-transfected ECs (Figure S8A). Secondly, miR-425-5p- or miR-scramble-transfected ECs were mixed in a Matrigel plug and transplanted into the back of immunodeficient mice for 3 days. Our results showed that, compared with miR-scramble-transfected ECs, miR-425-5p-transfected ECs displayed a statistically significant (1) increase in the number of viable ECs ($CD105^+CD144^+CD31^+$), and (2) decrease in the number of apoptotic ECs (Annexin V^+ $CD105^+CD144^+CD31^+$) cells (Figures 4B and S8B). Finally, compared with miR-scramble-transfected ECs, we showed a statistically significant increase in the number of human $CD31^+$ cells per area in the plugs of animals that were transplanted with miR-425-5p-transfected ECs (Figure 4C). Overall, our results showed that, similar to the results obtained *in vitro*, transfection of ECs with miR-425-5p enhanced their survival in an *in vivo* Matrigel plug assay.

Modulation of sEVs with miR-425-5p

Upon confirming the *in vivo* pro-survival effect of miR-425-5p in ECs, we evaluated its functional role in a type I diabetic wound healing mouse model. Diabetes is associated with impaired peripheral vasculature due to the presence of dysfunctional ECs.[28–30] One of the current approaches for treating diabetic ulcers is to restore the blood supply to the affected area, which requires an induction of EC survival, migration, and proliferation.[31] First, we showed that miR-425-5p was downregulated in wounds, both in wild type (WT) as well as a streptozotocin (STZ)-induced diabetic wound healing mouse model (Figure S9A). Next, we showed that topical administration of 200 pmol of miR-425-5p using RNAiMax (delivered immediately after wound induction) led to an acceleration in wound closure during a period of 10 days, with a statistically significant difference at days 3, 5, and 7 (Figure S9B). Based on these observations, and considering the translational potential of this therapy, we decided to explore the possibility of using sEVs as a delivery vehicle for miR-425-5p. We used sEVs secreted from human umbilical cord blood mononuclear cells (hUCBMNCs) because these cells are easily obtained from multiple stem cell banks and previous studies have demonstrated the regenerative potential of sEVs secreted from these cells in the context of diabetic wound healing.[32] sEVs were isolated from hUCBMNC using a standard differential ultracentrifugation protocol[32] followed by their characterization by transmission electron microscopy (TEM), nanoparticle tracking analysis (NTA), and phase analysis light scattering (PALS) analyses. Our results demonstrated the presence of extracellular vesicles (EVs) with size (~115 nm) and shape (cup-like) compatible with those of sEVs

presented as mean ± SD (n = 2 biological replicates; each biological replicate containing three independent technical replicates). (D) Confirmation of PTEN as a direct target of miR-425-5p and miR-5692c. Luciferase reporter assay confirmed a direct interaction between miR-425-5p and miR-5692c with the 3′ UTR of PTEN mRNA. Cells transfected solely with the reporter were used as control. Results are mean ± SD (n = 6 independent technical replicates). Statistical analysis was performed by an unpaired t test. (E–G) Activation of pro-survival signaling pathways (E) PTEN, (F) AKT, and (G) ERK1/2 after the transfection of $CD34^+$-derived ECs with miR-425-5p or miR-5692c, as confirmed by Western blot analyses. Lipofectamine-treated cells were used as a control. GAPDH was used as a loading control. Bars represent mean ± SD of at least three biological replicates with two technical replicates. Statistical analyses were performed by a one-way ANOVA followed by a Tukey's multiple comparison test. $^*p < 0.05$, $^{**}p < 0.01$, $^{***}p < 0.001$, and $^{****}p < 0.0001$.

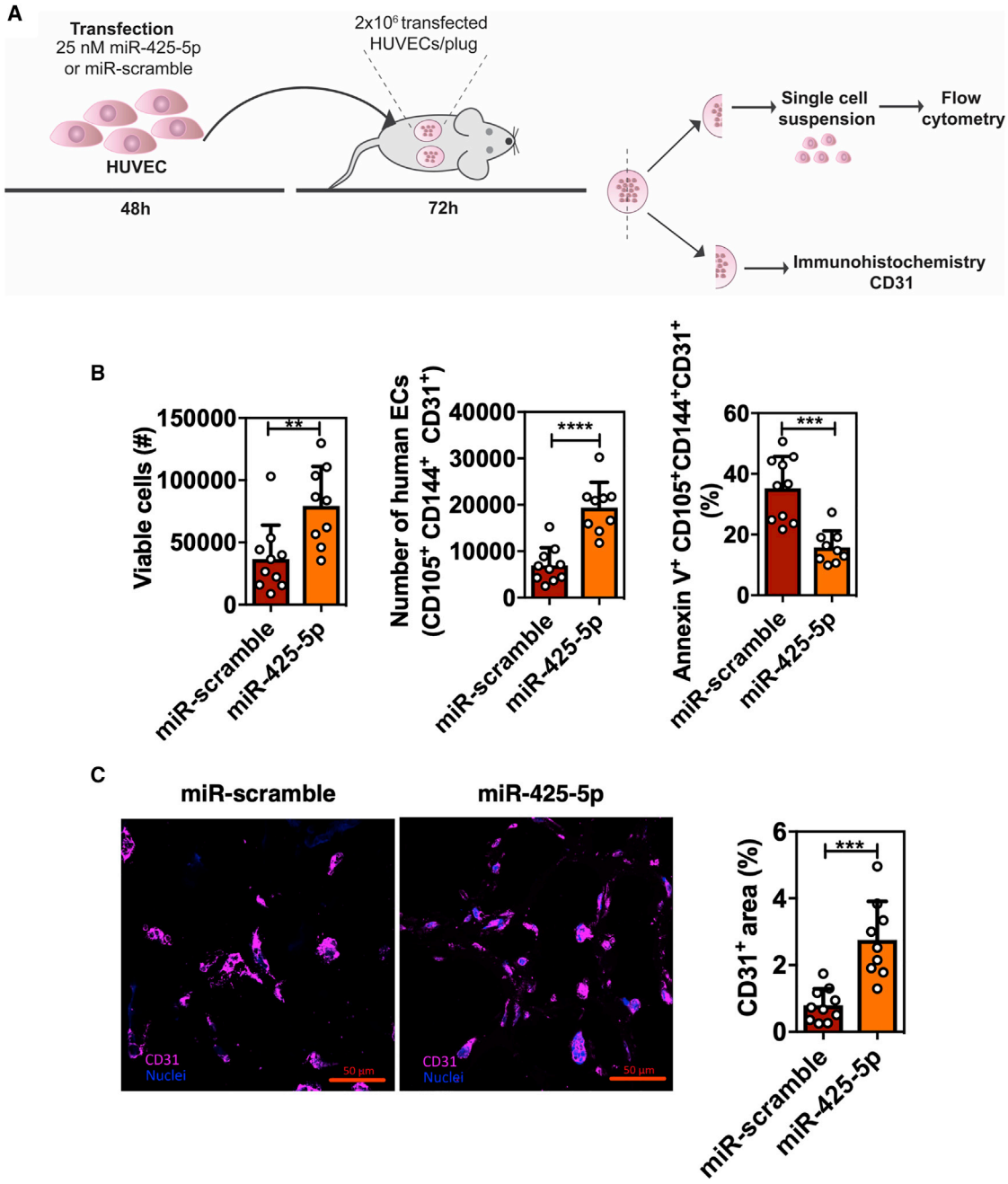

Figure 4. *In vivo* validation of the pro-survival effect of miR-425-5p

(A) Schematic overview of the *in vivo* Matrigel plug assay. HUVECs were transfected with 25 nM miR-425-5p for 48 h. After transfection, cells were mixed with Matrigel (2×10^6 cells/plug) and transplanted into the back of immunodeficient mice for 3 days (two plugs per mouse). After 3 days, animals were sacrificed, plugs retrieved, and half of the plug was processed for immunohistochemical analyses, whereas the other half was digested to obtain a single-cell suspension. Results are mean ± SD (n = 5 animals/group; two plugs per animal). Statistical analysis was performed by an unpaired t test. $^{**}p < 0.01$, $^{***}p < 0.001$, and $^{****}p < 0.0001$. (B) Total number of viable cells, total number of human ECs (based on the expression of specific surface markers such as CD105, CD144, and CD31), and percentage of apoptotic human ECs (based on Annexin V staining) were analyzed. (C) The expression of CD31 was quantified in the plugs retrieved from the animals and the total area of CD31 was quantified. Results are mean ± SD (n = 5 animals/group; two plugs per animal). Statistical analysis was performed by an unpaired t test. $^{***}p < 0.001$.

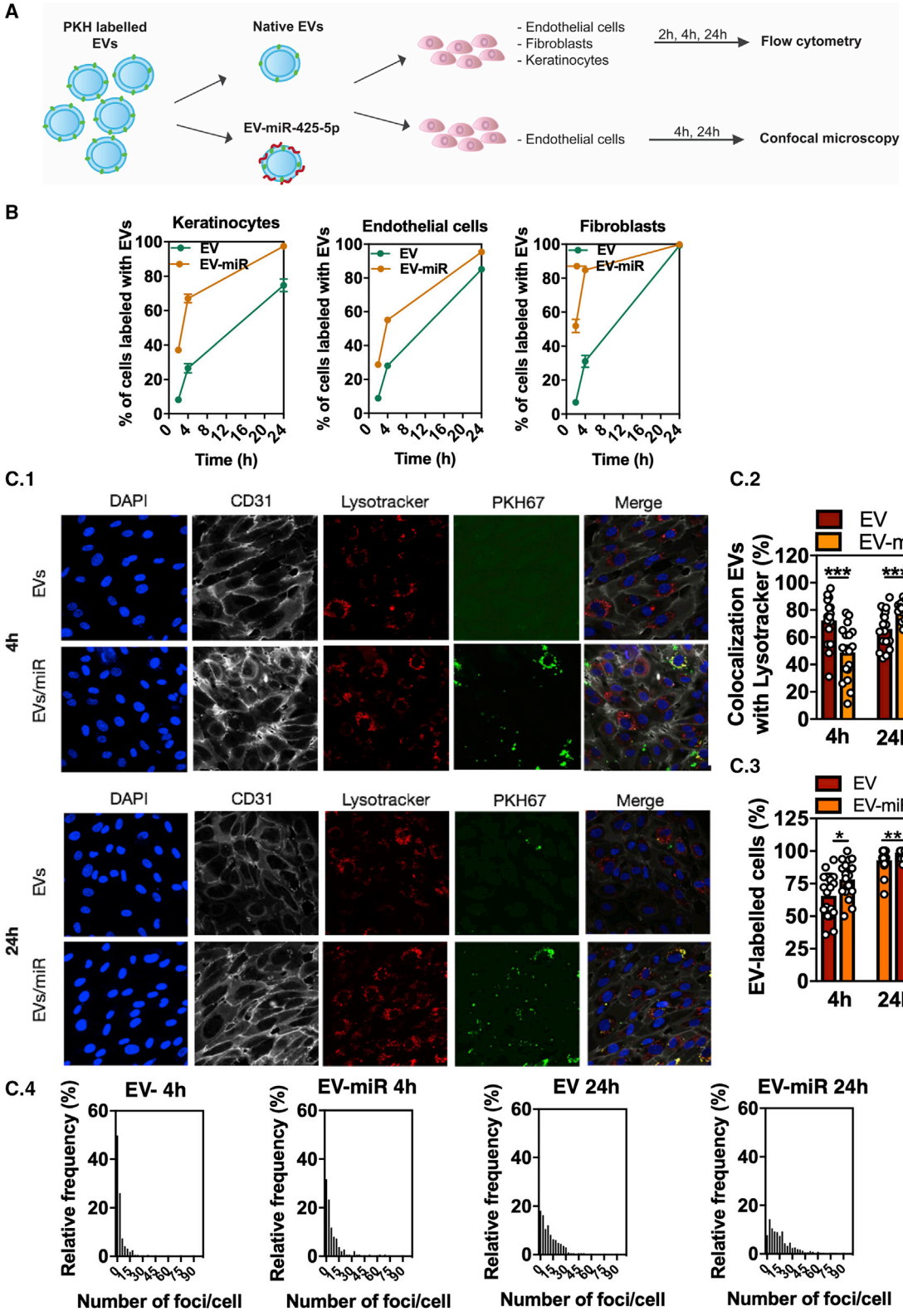

(legend on next page)

(Figures S10A–S10C). Next, sEVs were modulated with miR-425-5p or miR-scramble using Exo-Fect,[19] and our results showed a statistically significant increase in the expression of miR-425-5p in modulated versus native EVs (>30,000 upregulation; Figure S10D). Similar to the results obtained upon transfection of ECs with miR-425-5p using RNAiMax, treatment of ECs with miR-425-5p-modulated sEVs, but not native sEVs, enhanced the survival of ECs exposed to ischemic conditions (Figure S10E). Overall, our results showed that miR-425-5p is downregulated in diabetic and non-diabetic wound healing and that the topical delivery of miR-425-5p by Lipofectamine accelerated healing. Furthermore, we showed that sEVs may be modulated with miR-425-5p and the miR-425-5p-modulated sEVs were able to enhance the survival of ECs exposed to ischemic conditions.

Uptake and intracellular trafficking of sEVs enriched with miR-425-5p by skin cells

The internalization of native and miR-425-5p-modulated sEVs was performed in cell types known to play a role in wound healing: keratinocytes, ECs, and fibroblasts (Figures 5 and S11). For this purpose, sEVs were labeled with PKH67, a fluorescent membrane amphiphilic dye commonly used to label sEVs.[33,34] Previous results obtained by us indicated that PKH67 did not fluoresce in the absence of sEVs and that the presence of Exo-Fect in the sample did not alter sample fluorescence, prior to cell administration.[19] Herein we showed that both PKH67-labeled native and miR-425-5p-modulated sEVs were highly (more than 90% of the cells had sEVs after 24 h) taken up by all the three cell types (Figures 5B and S11). In addition, the internalization of miR-425-5p-modulated sEVs was faster in fibroblasts and keratinocytes than ECs but reached a similar steady state at 24 h for all the cell types (Figure 5B). Moreover, although the number of ECs transfected with sEVs at 2 and 4 h was lower than the other cell types, the number of sEVs per cell was larger in ECs (see the fluorescence intensity in Figure S11). Finally, our results showed that, for all three cell types, the internalization of miR-modulated sEVs was higher than native sEVs, particularly after 2 or 4 h of exposure.

To further confirm the cellular uptake and evaluate the intracellular trafficking of native and miR-modulated sEVs, we performed confocal microscopy. ECs were incubated with PKH67-labeled native or miR425-5p-transfected sEVs for 4 and 24 h and subsequently the cells were labeled with 4',6-diamidino-2-phenylindole (DAPI) (nuclei), CD31 (endothelial cell membrane), and LysoTracker red (lysosomes). sEV internalization was evaluated by the number of ECs that had sEVs (green fluorescence) relative to the total number of cells labeled with CD31 (Figure 5C). Approximately 77% of ECs internalized miR-425-5p-modulated sEVs after 2 h, while only 64% internalized native sEVs. In addition, cells treated with miR-425-5p-modulated sEVs had higher fluorescence than cells treated with native sEVs, indicating that the number of sEVs per cell was higher in miR-425-5p-modulated sEVs (Figure 5C). Our results further showed that the co-localization between labeled sEVs and the lysosomal compartment (Lysotracker$^+$ compartment) was similar at 4 h and slightly higher for miR-425-5p-modulated sEVs than native sEVs at 24 h. These results demonstrated that a significant percentage of native and miR-425-5p-modulated sEVs were within the cell. Altogether, our results showed that miR-425-5p-modulated sEVs were internalized by the three skin cell types tested (i.e., ECs, fibroblasts, and keratinocytes), although with differences in terms of kinetics and number of sEVs per cell. In addition, compared with native sEVs, our miR-425-5p-modulated sEVs were more efficiently internalized by all cell types.

Bioactivity of sEVs enriched with miR-425-5p in a diabetic skin wound animal model

To evaluate the functional role of miR-425-5p-modulated sEVs in the STZ-induced diabetic wound healing mouse model, we topically administered, bidaily, miR-425-5p- or miR-scramble-modulated sEVs (per day: 0.2 μg of sEVs transfected with 4 pmol of miR-425-5p or miR-scramble) on the wounds (Figure 6A). Our results showed that miR-425-5p-modulated sEVs significantly accelerated wound closure during a period of 10 days, with a statistically significant difference at days 3, 5–7, and 9 (Figure 6B). At days 2 and 5, there was a statistically significant increase in the expression of miR-425-5p in the wound area compared with the control (miR-scramble-treated wounds; Figure 6C). Importantly, at day 5, our results showed a statistically significant increase in the number of CD31$^+$ lumens (i.e., vessels lined by cells expressing the endothelial marker CD31) into the wound area for mice treated with miR-425-5p-modulated sEVs compared with miR-scrambled-modulated sEVs mice (Figure 6D).

Animals treated with miR-425-5p-modulated sEVs displayed improved wound re-epithelialization at day 5 compared with control (Figure 7A). The wound edge and epithelial gap were similar between animals treated with miR-scramble- and miR-425-5p-modulated sEVs, indicating no difference in wound contraction over that period (Figures 7A1 and 7A2). The re-epithelialization percentage (i.e., the ratio of proliferative front over wound edge) was statistically significantly higher in the miR-425-5p-modulated sEV group than in

Figure 5. Uptake and intracellular trafficking of native and miR-modulated sEVs

(A) Schematic overview of the assays performed to study the uptake and internalization of native and miR-modulated sEVs by skin cells (ECs, fibroblasts, and keratinocytes). (B) Cellular uptake of PKH67-labeled sEVs loaded with miR-425-5p. Keratinocytes, ECs, and fibroblasts were incubated with PKH67-labeled native or miR-425-5p-modulated sEVs for 2, 4, and 24 h and the cellular uptake was evaluated by flow cytometry. Results are mean ± SD (n = 3 biological replicates). Statistical significance was evaluated by a two-way ANOVA followed by a Bonferroni post test. *$p < 0.05$, ***$p < 0.001$. (C) ECs were incubated with PKH67-labeled native or miR-425-modulated sEVs for 4 and 24 h and analyzed by confocal microscopy (C.1). The percentage of co-localization between PKH67-labeled sEVs (green) and LysoTracker red (labeling the endolysosomal compartment) was quantified (C.2) and the foci number and distribution measure for each time point (C.3). Results are mean ± SD (n = 3 technical replicates; for each replicate, four images were taken for quantification purposes). Statistical analysis was performed by an unpaired t test, where *$p < 0.05$ and ***$p < 0.0001$. Bar corresponds to 50 μm.

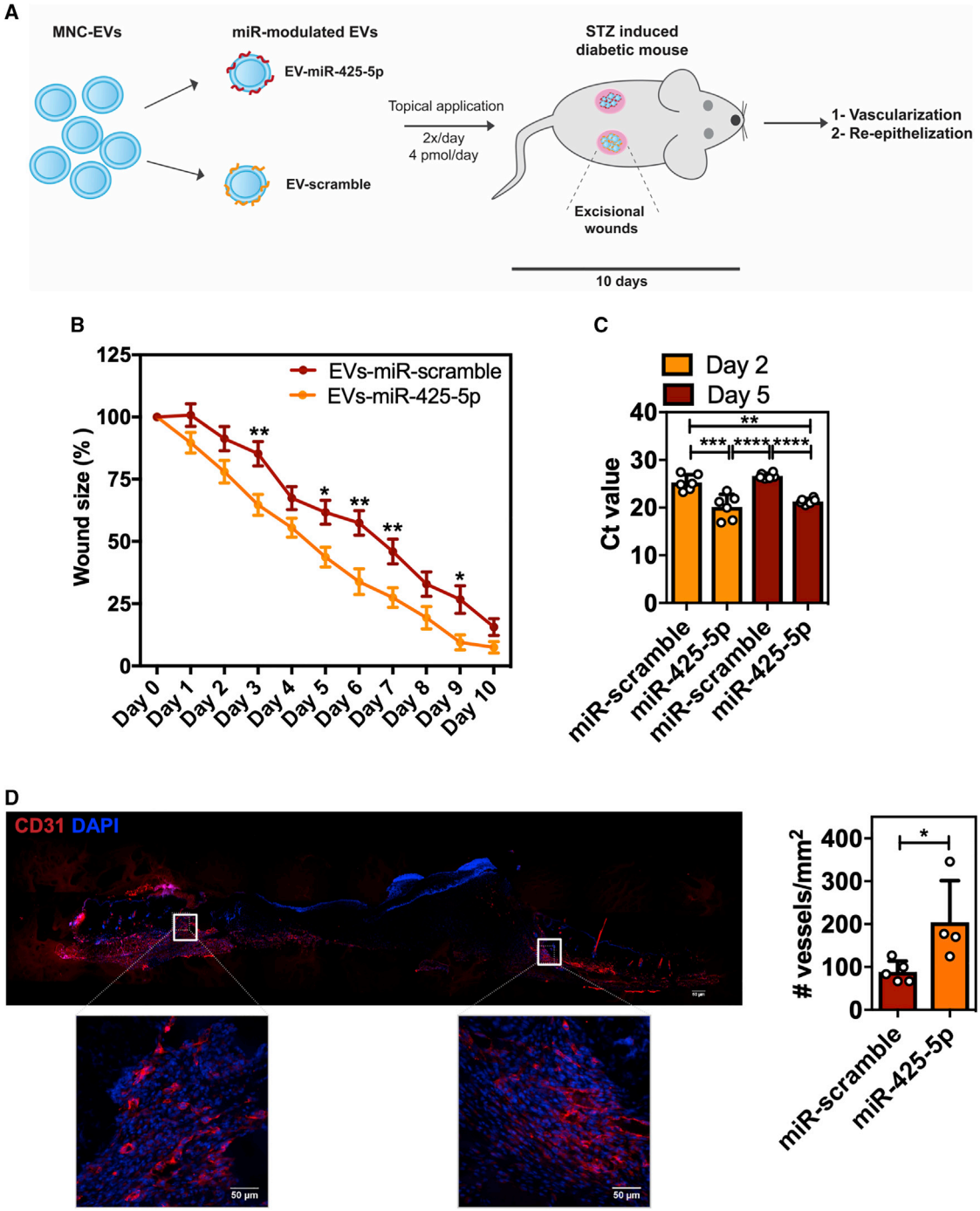

Figure 6. miR-425-5p-modulated sEVs enhanced *in vivo* healing of type I diabetic chronic wounds by increasing vascularization

(A) Schematic overview of the methodology used to modulate sEVs isolated from umbilical cord blood-derived mononuclear cells with miR-425-5p and evaluate their effect on wound healing using an STZ-induced diabetes wound healing mouse model. Mice were treated bidaily, topically, with 0.2 µg of sEVs transfected with 4 pmol of miR-425-5p or miR-scramble. (B) Percentage of wound area after topical treatment with miR-425-5p-modulated sEVs or miR-scramble-modulated sEVs applied onto type I diabetic chronic wounds. Results are average ±SEM (n = 6 mice per group; 12 wounds per group). Statistical analysis was performed by an unpaired t test. (C) Quantification by qRT-PCR of the expression of miR-425-5p after topical administration of miR-scramble- or miR-425-5p-modulated sEVs. Total RNA was isolated at day 2 and 5 from the wound area of STZ-induced diabetic mice. Results are mean ± SEM (n = 5 mice for miR-scramble and n = 6 mice for miR-425-5p-modulated sEVs). Statistical analyses were

(legend continued on next page)

control (Figure 7A3). Next, we evaluated the properties of the epithelial tongue; i.e., the first layer of keratinocytes covering the wound bed. The epithelial thickness and fluorescence of the advancing epithelial tongue was significantly larger in animals treated with miR-425-5p-modulated sEVs than control (Figures 7B1 and 7B2). Moreover, the proliferative front and proliferative edge area were superior in animals treated with miR-425-5p-modulated sEVs than control (Figures 7B3 and 7B4). Overall, our results showed that administration of miR-425-5p-modulated sEVs into the wounds of STZ-induced diabetic mice enhanced wound healing partially by accelerating wound vascularization and re-epithelialization.

DISCUSSION

Survival, migration and proliferation of ECs is crucial for tissue regeneration in several (patho)physiological contexts. Unfortunately, upon injury, the local pro-inflammatory and ischemic environment often hinder EC survival, migration and proliferation, culminating in poor regeneration and restoration of tissue function.[35] Using high-throughput screening analysis, we identified 25 miRs capable of enhancing the survival of ECs exposed to ischemia-mimicking conditions (0.1% O_2 and growth factors and serum-depleted media). Besides increasing survival, two of the identified miRs (miR-425-5p and miR-5692c) stimulated EC migration *in vitro* and one of them (miR-425-5p; conserved across species) increased the survival of ECs transplanted *in vivo*. Moreover, we developed a clinically relevant strategy, based on the modulation of sEVs with miR-425-5p (used as a proof of concept) for *in vivo* delivery. Finally, we showed that the delivery of miR-425-5p-modulated sEVs enhanced wound closure in diabetic mice, compared with the control (miR-scramble-modulated EVs), partially by enhancing wound angiogenesis.

EC survival, rather than EC proliferation or migration, was selected as the main readout in the high-content screening (HCS) because the impact of EC survival in tissue regeneration is poorly investigated and the readout was relatively easy to implement in an HCS assay. However, it should be noted that biomolecules able to interfere with EC survival may also affect other EC functions, such as migration and proliferation. EC survival involves a myriad of different signaling pathways that activate pro-survival/proliferative cascades and/or inhibit genes known to negatively regulate survival and/or proliferation. Previous strategies to increase EC survival included the use of pro-angiogenic growth factors or proteins[36] as well as small molecules.[37] However, given the multifactorial nature of EC survival, a multitarget approach is likely required to improve cell survival, as reported in other cell types.[38] Therefore, we have used a miR-based approach to target multiple targets at the same time. Previous studies reported miRs that have contributed for EC survival, such as miR-26b,[13] miR-148a-3p[39] and miR-17.[12] However, to the best of our knowledge, no study has used HCS to identify pro-survival miRs; i.e., an assay in which the main readout was survival and not EC proliferation.[13] Therefore, the current study identifies, for the first-time, pro-survival miRs that may be relevant in the context of endogenous tissue regeneration, particularly in ischemic conditions, or to enhance the survival and/or engraftment of transplanted exogenous ECs. Importantly, although beyond the topic of this manuscript, we have also identified miRs that are able to induce a cell death program in stressed ECs and that may be valuable in other diseases, such as the ones related to chronic inflammation.[35]

ECs and endothelial progenitor cells (EPCs) are critical for a successful regenerative program in many tissues. In the context of skin, an adequate vascularization and blood supply is paramount for the survival and growth of skin tissue after injury. Previously, we have shown that the transplantation of ECs and EPCs, with an enhanced survival program, was important for the skin regenerative program in a diabetic wound healing animal model.[23] Other studies have also confirmed that the transplantation of ECs, reprogrammed with a pro-survival program, in murine diabetic wounds potentiated skin healing.[40] In the current study, we investigated the *in vivo* pro-survival program of the miR-425-5p using a Matrigel plug assay. Our results clearly showed that ECs transfected with miR-425-5p had enhanced survival. In addition, our results demonstrated that the topical delivery of miR-425-5p-modulated sEVs in skin diabetic wounds enhanced their healing through increased neovascularization and re-epithelialization. Therefore, it is likely that miR-425-5p-modulated sEVs acted in different skin cells and not only in ECs. Indeed, our *in vitro* studies showed that modulated sEVs were readily internalized by keratinocytes and fibroblasts, besides ECs. Further studies are necessary to unravel the role of miR-425-5p in other cell types, such as, for example, immune cells, both *in vitro* as well as *in vivo*. Recently, it has been shown that sEVs isolated from epidermal stem cells, which contained miR-425-5p as one of the lumen components, were able to reduce scar formation in rat skin wound healing by inhibiting the differentiation of dermal fibroblasts into myofibroblasts.[41]

Mechanistically, we showed that both miR-425-5p and miR-5692c shared a transcriptomic signature that ultimately culminated in enhanced EC survival *in vitro*. Our transcriptomic analysis followed by a validation experiment using siRNAs against the putative targets of miR-425-5p showed that knockdown of *DACH1*, *PTEN*, *RGS5* and *VASH1* phenocopied the pro-survival effects of miR-425-5p in ECs. *PTEN* inhibition, as mentioned before, is a well-known mechanism leading to enhanced survival via activation of the AKT signaling pathway. *DACH1* (Dachshund homolog 1) is a transcription factor previously reported to be involved in coronary artery growth and protection against cardiac injury.[42,43] *RGS5* (regulator of G-protein signaling 5) inhibits signal transduction by increasing the GTPase activity of G-protein alpha subunits, thus inactivating them in their

performed by a one-way ANOVA followed by a Tukey's multiple comparison test. **$p < 0.01$, ***$p < 0.001$, and ****$p < 0.0001$. (D) Number of vessels ($CD31^+$-positive vessels) per area in excisional wounds at day 5 upon treatment with miR-scramble- or miR-425-5p-modulated sEVs. Results are mean ± SD (n = 5 mice for miR-scramble and n = 4 mice for miR-425-5p-modulated sEVs). Statistical analysis was performed by an unpaired t test. *$p < 0.05$.

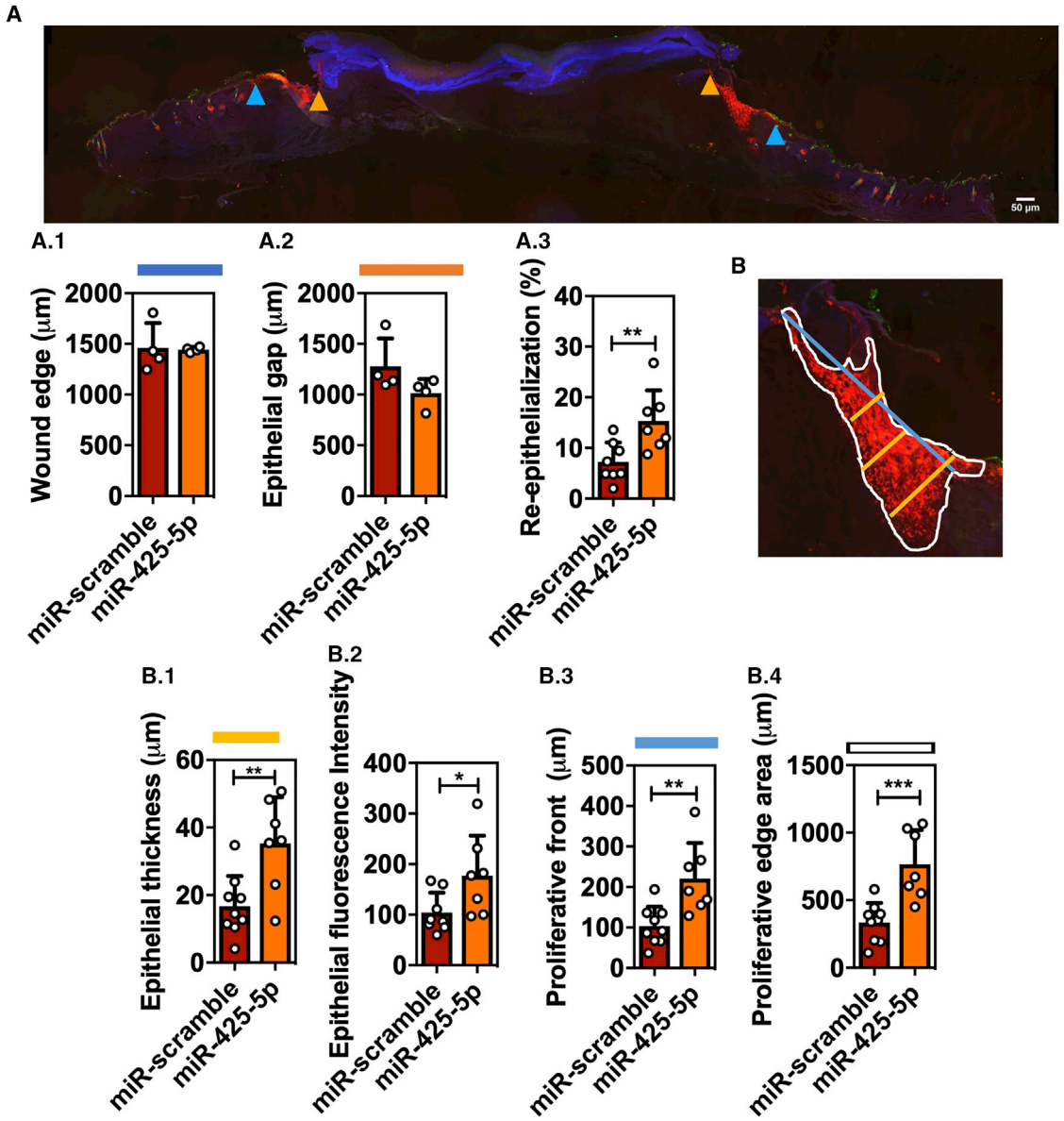

Figure 7. miR-425-5p-modulated sEVs enhanced *in vivo* healing of type I diabetic chronic wounds by increasing re-epithelialization

(A) Representative immunofluorescence image of a wound treated with miR-425-5p-modulated sEVs at day 5. Blue arrowheads indicate wound edges; orange arrowheads indicate the tips of the healing epithelial tongue (epithelial gap). The tips of the healing epithelial tongue were identified by the expression of keratin 14 (red). Scale bar corresponds to 50 µm. (A.1–A.3) Quantification of wound edge (A.1), epithelial gap (A.2), and re-epithelialization (A.3). (B) Representative image of an epithelial tongue; 40× magnification of the right-side tongue from (A). Epithelial thickness (B.1), epithelial fluorescence intensity (B.2), proliferative front (B.3), and proliferative edge area (B.4) were calculated on both sides of each lamina based on the expression of keratin 14 (red). Results are mean ± SD (at least n = 4 mice per condition). Statistical analysis was performed by an unpaired t test. *$p < 0.5$, **$p < 0.01$, and ***$p < 0.001$.

inactive GDP-bound form. Interestingly, *RGS5* is highly expressed in vessels and its knockdown was shown to activate ECs and modulate EC mediated inflammation.[44] Moreover, it was shown that *RGS5*, although not other RGS family members, were induced in hypoxia-exposed ECs and *RGS5* knockdown attenuated apoptosis in ECs.[45] *VASH1* (tubulinyl-Tyr carboxypeptidase 1) is a tyrosine carboxypeptidase that removes the C-terminal tyrosine residue of alpha-tubulin and thus suppresses angiogenesis *in vitro* and *in vivo*.[46] Strikingly, compared with WT mice, $VASH1^{-/-}$ mice lived longer and presented a milder senescence phenotype, a mechanism partially regulated by insulin signaling.[47] Overall, the putative targets identified have been previously involved in EC function/activity, but their role as pro-survival genes in ECs exposed to ischemia-mimicking conditions has not been described.

The advantages of using native and engineered sEVs for the *in vivo* delivery of therapeutic compounds, in particular miRs, has been recently discussed by us and others.[48,49] The most commonly used strategy to modify sEVs with a molecule of interest relies on the genetic modification of the secreting cell followed by the isolation of sEVs from the supernatant. However, the clinical potential of this approach is rather limited given the risks associated with the genetic modification procedures (i.e., use of virus to insert the template of interest into the secreting cell), the low sEV yield, the high costs associated with cell culture in good manufacturing practices (GMP) conditions and the batch-to-batch variability. Thus, methods capable of inserting the same molecule post sEV isolation are much needed. Recently, we compared the different post-isolation methods reported in the literature and showed that Exo-Fect, a commercial agent, was superior to the other methods (electroporation, heat-shock, cholesterol conjugation, and detergent permeabilization) to modulate sEVs, regardless of their source, with pre-selected miRs.[19] Of note, we previously used a reporter cell line to evaluate the functional delivery of sEVs modulated with miRNAs and Exo-Fect and showed that Exo-Fect incubated with a selected miR, in the absence of sEVs, was unable to elicit a functional response, suggesting that the effects were mediated by the complexation of the miR with the sEVs and not due to the formation of artifacts between Exo-Fect and the miR.[19] Exo-Fect has previously been used to modulate sEVs with miRs, followed by *in vivo* delivery, in the context of obesity,[50] cancer[51] and neurosciences.[52] However, the current study is the first to evaluate the topical administration of miR-modulated sEVs in the context of skin wound healing. It is important to note that the level of miR enrichment obtained in Exo-Fect-modulated sEVs is more than 2^{10}-fold compared with native sEVs. This enrichment strategy is much higher (25-fold) than the one reported for the electroporation of sEVs[18] that has recently been reported in skin diabetic wound healing.

Several advanced interventions have been evaluated in diabetes-impaired wound healing animal models with variable efficacy, such as biomaterials, biomolecules (e.g., miRs, mRNA, small molecules), stem cells, non-cellular products (e.g., sEVs), as well as tissue engineering products. The comparison between the different skin wound healing studies is far from trivial given the differences in the animal species (mostly mice and rats), models (high-fat diet, chemically versus genetically induced diabetic mice), wound type (excisional versus non-excisional), sEV origin, dose, and delivery route, as well as approaches to evaluate/quantify healing (wound area based on histological scores or photography, immunohistochemical analysis for pre-determined parameters, among others). The wound closure results of our formulation were compared against a US Food and Drug Administration (FDA)-approved formulation based on platelet-derived growth factor-NN ($PDGF_{BB}$), previously reported by us in the same animal model.[32] Our results showed that wounds treated with a daily dose of $PDGF_{BB}$ (i.e., 8 μg of the growth factor per cm^2 of wound; concentration recommended by the vendor Regranex) had an average size that corresponded to 88% at day 5, and 28% at day 10, of the initial wound size, while wounds treated with miR-425-5p-modulated EVs had an average size that corresponds to 44% at day 5, and 8% at day 10, of the initial wound size. In addition, the current results compared favorably with the ones obtained recently by us in the same animal model using native UCBMNC-derived sEVs. In previous results, ∼50% of the wound area was opened after 7 days following a bidaily administration of native sEVs, whereas in wounds treated with miR-425-5p-modulated sEVs, only ∼25% of the wound area was opened at the same time point.[32] Moreover, the results reported here are promising compared with the skin healing scores obtained in animals treated with sEVs from different sources, either enriched or not for specific biomolecules (Table S12), or from other type of advanced therapies such as peptide-coated dressings[53,54] or injectable microporous gel scaffolds.[55]

In conclusion, we developed a platform, based on high-throughput screening and cellular assays involving ECs exposed to stress conditions, capable of identifying pro-survival miRs. Moreover, after identifying and validating the role of selected pro-survival miRs *in vitro* and *in vivo*, we develop a platform, based on the modulation of sEVs with the selected miRs, that has a high clinical potential to deliver therapeutic cargos *in vivo*. In addition to modulating the bioactivity of sEVs, future work will focus on strategies to selectively target a cell of interest *in vivo* and novel methodologies to modulate sEVs with miRs of interest. Moreover, despite the promising results obtained with miR-425-5p-modulated EVs, further work should be done to unravel the molecular mechanism of action *in vivo*.

MATERIALS AND METHODS

Isolation of $CD34^+$ cells from umbilical cord blood

For the collection of human umbilical cord blood, all donors signed an informed consent form in compliance with Portuguese legislation and the collection was approved by the ethical committee of Centro Hospitalar e Universitário de Coimbra (HUC-01-11). Human $CD34^+$-derived ECs were derived as previously described.[23] In brief, umbilical cord blood was collected, stored, and transported to the laboratory in sterile collection bags containing anticoagulant solution (citrate-phosphate-dextrose). All samples were processed within 48 h. Mononuclear cells (MNCs) were isolated by density gradient separation (Lymphoprep, StemCell Technologies SARL, Grenoble, France) and cryopreserved in a solution consisting of fetal bovine serum (FBS):Iscoveś Modified Dulbeccoś Medium:DMSO (55:40:5; % v/v) until further use.

Differentiation of $CD34^+$ cells into ECs

Following isolation, $CD34^+$ cells were seeded onto 1% (w/v) porcine skin type A gelatin-coated plates at 1×10^5 cells/cm^2 in endothelial growth medium (EGM-2; Lonza, Gaithersburg, MD, USA) supplemented with 50 ng/mL $VEGF_{165}$ (PrepoTech, Rocky Hill, USA) and 20% (v/v) FBS at 5% CO_2 and 37°C. After 15–20 days of culture, the presence of endothelial markers was confirmed by ICC and flow cytometry and the functionality of the obtained population assessed (see Pedroso et al.[23] for further details).

HCS assay: Protocol

$CD34^+$-derived ECs were seeded onto 1% (w/v) porcine skin type A gelatin-coated 96-well plates (Costar) at 1×10^4 cells/well in EGM-2 medium without antibiotics and left to adhere overnight. The next day, cells were transfected with a library of miR mimics (Dharmacon miRIDIAN miR Library, human mimic miRBase version 19.0; 2080 miR mimics) according to the manufacturerś instructions. Briefly, complexes of miR:Lipofectamine RNAiMAX (50 nM miR: 0.3 μL of Lipofectamine final concentration per well) were prepared in EBM-2 medium and allowed to form for 30 min at room temperature while gently rocking and then added to the cells. Transfection was allowed to proceed for 48 h after which medium was replaced by EBM-2 medium containing 1% (v/v) penicillin/streptomycin and plates were transferred to a hypoxia chamber (0.1% O_2, hereafter denoted as ischemic conditions) and cultured for a further 48 h. Per plate, untreated and Lipofectamine-treated cells were used as a control. The screening was repeated twice using two different pools of $CD34^+$-derived ECs (each pool consisting of a mixture of five different donors). After 48 h in ischemic conditions, medium was discarded, the cell layer was washed twice with PBS (200 μL), and fixed with 4% (v/v) paraformaldehyde (PFA) at room temperature. Next, cells were incubated with Hoechst 33342 (1 μg/mL; Sigma-Aldrich) for 30 min at 37°C and image acquisition was performed immediately (see details below).

HCS assay: Image acquisition and analyses

Image acquisition was performed using an automated high-content imager (InCell Analyzer 2200; GE Healthcare) at 20× magnification. A total of eight randomly selected bright-field and fluorescent (nuclear staining) images were acquired per well and total nuclear count was performed using the InCell Investigator (GE Healthcare). An miR was identified as a hit if (1) the total number of cells was higher than the mean plus two times the standard deviations of the Lipofectamine-treated cells. and (2) it was present on both replicates of the screening. Hereinafter, miRs that met these criteria are referred to as pro-survival miRs.

HCS assay: Hit validation assays

To confirm the results obtained in the primary screening, we re-tested the 25 miRs identified therein using $CD34^+$-derived ECs and the same experimental procedures (n = 3 per miR). After confirming the pro-survival effect of the miRs, we further tested two of them (miR-425-5p, previously identified as a pro-survival miR, and miR-5692c) using well-established EC models, namely HUAECs and HUVECs. HUVECs and HUAECs were obtained from Lonza and cultured in EGM-2 medium according to the manufacturerś instructions. $CD34^+$-derived ECs, HUVECs, and HUAECs were plated as described above and three miR concentrations (10, 25, and 50 nM) were tested in triplicate for their capacity to enhance cell survival in ischemic conditions. To account for differences in cell numbers we performed nuclear staining before transferring the plates to the hypoxia chamber and that value was used to calculate the survival percentage after culturing the cells in ischemic conditions for 48 h. Image acquisition and analysis was performed as described above with a small modification of the original protocol. In brief, the total number of death cells was calculated based on an image-based segmentation strategy, whereas condensed nuclei were considered as death cells.

Characterization of transfected ECs: Angiogenesis assay

$CD34^+$-derived ECs were seeded onto 1% (w/v) porcine skin type A gelatin-coated six-well plates at 2×10^5 cells/well in EGM-2 medium without antibiotics and left to adhere overnight. Transfection was performed by preparing complexes as described above (25 nM miR and 6 μL of Lipofectamine RNAiMAX per well). Transfection was allowed to proceed for 48 h, after which cells were harvested with TripLE express, counted, and 1×10^4 cells were seeded onto Ibidi μ-slides pre-coated with Matrigel (10 μL/well) in EBM-2 medium (50 μL) containing 1% (v/v) gentamycin according to the manufacturerś instructions. Cells cultured in EBM-2 medium supplemented with $VEGF_{165}$ (50 ng/mL; PrepoTech, Rocky Hill, USA) were used as a positive control. The assay was performed in normoxia as well as in hypoxia (0.1% O_2) and after 4 h, a bright-field image covering the area of the well was acquired as described above. Four independent wells were analyzed and the number of capillaries was determined by manually counting the number of completely formed capillary-like tubes.

Characterization of transfected ECs: Migration assay

$CD34^+$-derived ECs were seeded onto 1% (w/v) porcine skin type A gelatin-coated 96-well plates (Costar) at 1×10^4 cells/well in EGM-2 medium without antibiotics and left to adhere overnight. The following day, cells were transfected with 25 nM miR and transfection was allowed to proceed for 48 hafter which medium was discarded and cells were starved overnight in EBM-2 medium alone. The next day, wounds were created directly onto the 96-well plate by scratching the surface with a 200-μL pipette tip (Neubauer), the cell layer was washed with EBM-2 to remove unattached cells and EBM-2 medium containing 1% (v/v) gentamycin was added to the wells. Medium containing $VEGF_{165}$ (50 ng/mL; PrepoTech, Rocky Hill, USA) was used as positive control. The assay was performed in normoxia as well as in hypoxia (0.1% O_2) and after 24 h, one bright-field image was acquired as described above. Eight replicates per experimental conditions were performed and the percentage of wound area was determined using the following formula: (wound size after 24 h/wound size at 0 h) × 100.

Characterization of transfected ECs: Western blot analyses

$CD34^+$-derived ECs were seeded onto 1% (w/v) porcine skin type A gelatin-coated six-well plates at 1.5×10^5 cells/well in EGM-2 medium without antibiotics and left to adhere overnight. Transfection was performed as described above (25 nM miR and 6 μL of Lipofectamine per well) and allowed to proceed for 48 h, after which medium was removed and cells were washed with room-temperature PBS and lysed using RIPA buffer supplemented with protease/phosphatase inhibitor cocktail (150 μL, #5872, Cell Signaling Technologies). Cell lysates were centrifuged at 14,000 relative centrifugal force (RCF) for 15 min at 4°C and the supernatant was transferred to pre-cooled tubes and immediately stored at −80°C. Protein quantification was

performed using Pierce BCA Protein Assay Kit (#23225, Thermo Fisher Scientific) according to the manufacturerś instructions. Protein extracts (30 μg) were resolved in 8%–10% SDS-PAGE gels and transferred into polyvinylidene difluoride (PVDF) membranes for 90 min at 100 V. Membranes were blocked in 5% (w/v) bovine serum albumin (BSA) in tris buffered saline containig 2% Tween20 (TBST (0.2%)) and probed against PTEN (#9559 Cell Signaling Technology), AKT (#4691 Cell Signaling Technology), phosphorylated (Ser473)-AKT (#4060 Cell Signaling Technology), ERK1/2 (#4695 Cell Signaling Technology), phosphorylated (Thr202/Tyr204)-ERK1/2 (#4376 Cell Signaling Technology), and VE-cadherin (#sc-8999, Santa Cruz). Unless otherwise stated, all antibodies were used at a final dilution of 1:1,000 and incubated at 4°C overnight. Membranes were then incubated with secondary peroxidase-conjugated antibodies (1:10,000) for 1 h at room temperature. The specific detection of probed proteins was achieved by a chemiluminescence reaction using WesternBright Quantum HRP substrate (Advansta) according to the manufacturerś instructions.

Characterization of transfected ECs: RNA-seq analyses

$CD34^+$-derived ECs were transfected as described above. In brief, $CD34^+$-derived ECs (1.5×10^5 cells/well) were plated onto a six-well plate in triplicate and transfected with 25 nM of miR-425-5p or miR-5692c using Lipofectamine RNAiMAX (6 μL per well). Transfection was allowed to proceed for 48 h after which total RNA was isolated using the RNeasy kit (Qiagen) according to the manufacturerś instructions. RNA-seq was performed using the BGISEQ-500 platform (BGI, Hong Kong). In brief, RNA quantification was performed using a NanoDrop and the integrity was determined using the Bioanalyzer 2100 (Agilent). After quality control assessment, oligo (dT) magnetic beads were used to select mRNA with poly(A) tail and mRNA was sheared and reverse transcribed using random primers to obtain cDNA, which was used for library construction and subsequent sequencing. All the generated raw sequencing reads were filtered to remove reads with adaptors, reads in which unknown bases were more than 10% of the total, and low-quality reads. Clean reads were then obtained and stored as FASTQ format. Bowtie2 was used to map clean reads to the reference gene and HISAT was used to map to the reference genome. RSEM was used to quantify gene expression, and the normalized value of FPKM was used to calculate the expression level of each gene. Subsequently, the NOISeq method was used to calculate which genes were differentially expressed in our samples, and the results were presented as $\log_2$ FC between control and treatment. Heatmaps show centered and scaled log(FPKM +1) values for genes differentially expressed between miR-425-5p and miR-5692c and respective control (Lipofectamine-treated cells). For PCA, features were centered and scaled and the amount of variance of the first two components was plotted.

Characterization of transfected ECs: miR target validation by RT-PCR

Total RNA from miR-modulated $CD34^+$-derived ECs was extracted using the RNeasy kit (Qiagen, Hilden, Germany) according to the manufacturerś instructions. For the quantification of gene expression, total RNA was reverse transcribed using hexameric random primers and TaqMan reverse transcription reagents (Applied Biosystems, CA, USA). qRT-PCR for the putative miR target genes was performed using POWER SYBR Green PCR Master Mix (Applied Biosystems) and the detection was carried out in a 7500 Fast Real-time PCR System (Applied Biosystems). The housekeeping gene *GAPDH* was used for normalization, and FCs were determined using the $2^{-\Delta\Delta Ct}$ method.[56] Primer sequences are included in Table S1.

Characterization of miR-modulated ECs: ICC

For ICC, $CD34^+$-derived ECs were transfected with 25 nM miR and 48 h after transfection, cells were fixed with 4% (v/v) PFA for 15 min at room temperature and ICC staining was performed according to the antibody provider instructions. Briefly, VE-cadherin staining was performed after fixation, permeabilization with 0.1% (v/v) TritonX-100 and blocking with 3% (v/v) BSA for 1 h. Next, cells were incubated for 2 h at room temperature with the primary antibody for VE-cadherin (1:250; sc-9989, Santa Cruz Biotechnology), washed with PBS and incubated with the secondary antibody (1:500; AlexaFluor^{555} goat anti-mouse) for 1 h at room temperature. Nuclei were stained with Hoechst 33342 (1 μg/mL; Invitrogen) and images were acquired using the high-content imager as described above.

Characterization of miR-modulated ECs: *In vivo* murine Matrigel plug assay

This study was performed in compliance with Dutch government guidelines and Directive 2010/63/EU of the European Parliament. The animal experiment was approved by the animal welfare committee of the Leiden University Medical Center (approval reference number 116002016645). For the isolation of HUVECs, anonymous umbilical cords were obtained in accordance with guidelines set out by the Code for Proper Secondary Use of Human Tissue of the Dutch Federation of Biomedical Scientific Societies (Federa) and conforming to the principles outlined in the Declaration of Helsinki. Isolation and culturing of HUVECs was performed as previously described.[57] In brief, 3×10^6 HUVECs were seeded in 0.2% (w/v) gelatin (Sigma G1890)-pre-coated T75 flasks and grown in complete culture medium (EGM-2, Lonza) until they reached 80% confluence. HUVECs were transfected with Lipofectamine RNAimax (Thermo Fisher Scientific, 13778) and 25 nM miR-425-5p or miR-scramble (Qiagen, YM00471725-ADA and YM00479902) in EBM-2 medium (Lonza) according to the manufacturerś instructions. After 24 h, total RNA was isolated using the standard Trizol-chloroform extraction method and subsequently RNA was reverse transcribed using a high-capacity RNA to cDNA kit (Thermo Fisher Scientific). Transfection efficiency was analyzed 24 h after transfection by qRT-PCR using commercially available primers for miR-425-5p and U6 snRNA (Thermo Fisher Scientific, 001516 and 001973). For the *in vivo* Matrigel plug assay, HUVECs were transfected for 48 h, upon which the transfection medium was discarded and cells were washed with PBS, detached from the culture flask using trypsin-EDTA and counted.

Matrigel plugs for the *in vivo* study were prepared as follows: growth-factor-reduced Matrigel (BD Biosciences, 356231), in liquid form at 4°C, was mixed with 2×10^6 HUVECs transfected with miR-425-5p or miR-scramble in a final volume of 350 µL/plug. All the plugs were supplemented with recombinant human $VEGF_{165}$ (100 ng/mL; BioLegend, 583704).

In vivo EC survival was assessed in 11-week-old female immunocompromised Cby/cBy.Cg-fox1$^{<nu}$ mice (Charles River). Mice were anesthetized with isoflurane (induction 3.5%, maintenance 1.5%) and Matrigel plugs were injected into the subcutaneous space on the dorsal side of mice on both flanks (n = 5 mice/group, two plugs per mouse). At day 3, mice were euthanized via exsanguination, Matrigel plugs were removed, cut in half, and one-half was immediately snap frozen and stored at −80°C for immunohistochemical analysis (see details below), whereas the other half was weighed and stored in ice-cold cell recovery solution (Fisher Scientific, 354253). Single-cell suspensions were prepared by incubating the plugs for 2 h in the cell recovery solution at 4°C followed by mincing the plugs through a 40-µm cell strainer (BD Biosciences). Conjugated monoclonal antibodies to human CD31 (PECAM) brilliant violet 421 (303123), human CD144 (VE-cadherin) APC (348507), human CD105 (Endoglin) PE (323205), and Annexin V PE/Cyanine7 (640949), all acquired from BioLegend, were used to label the cells. Flow cytometry acquisition was performed on a BD LSR II flow cytometer (BD Biosciences). Data was analyzed using FlowJo V10.1 software (BD). Flow cytometry gating strategies with fluorescence minus one (FMO) controls (on single HUVECs) are shown in Figure S8B.

Characterization of miR-modulated ECs: Immunohistochemistry and quantification of CD31$^+$ cells in Matrigel plugs

Per plug, 5-µm frozen sections (five sections per Matrigel plug with a 30-µm distance between the sections) were fixed with ice-cold acetone and incubated with rat anti-human CD31 (1:100; Brilliant Violet 421; 03123 BioLegend) and the nuclear stain Oxazole yellow (1: 31000; SML-1792; Sigma). As a control, isotype antibody (Ig1,k BioLegend) was used. After overnight incubation, the sections were mounted with prolong Gold (Thermo Fisher). Per Matrigel plug, three pictures were taken with the confocal laser scanner microscope (Zeiss LSM 700) and the percentage of CD31$^+$ area/plug was quantified using FIJI ImageJ.

PTEN 3′ UTR luciferase assay

A plasmid containing the PTEN 3′ UTR with the predicted seed sequences for both miR-425-5p and miR-5692c and luciferase assay reagents were purchased from Active Motif. HeLa cells were seeded into 96-well plates at 7,500 cells/well in Dulbecco's modified Eagle's medium (DMEM) supplemented with 10% (v/v) FBS. The following day, cells were co-transfected with 12.5 ng of 3'UTR PTEN plasmid and 25 nM miR using Lipofectamine 2000 (ratio of 1:1:2 per well, respectively). After 24 h, medium was discarded and DMEM supplemented with 10% FBS was added to the wells. Luciferase assay was performed according to manufacturer's instructions. Luciferase signal was measured using a luminometer.

Isolation of sEVs

hUCBMNCs, isolated and stored as described above, were thawed in warm X-VIVO medium and immediately treated with DNAse I to degrade DNA arising from death cells (due to the freeze-thawing process). Subsequently, cells were centrifuged at 300 × *g* for 5 min and 2×10^6 cells/mL were cultured in X-VIVO 15 serum-free cell-culture medium (Lonza) supplemented with 100 ng/mL Flt-3 and 100 ng/mL stem cell factor (both from PeproTech) under hypoxia conditions (0.5% O_2) for 18 h. sEVs were purified from the conditioned medium (CM) by differential centrifugation as previously described.[58] In brief, CM was collected and centrifuged at 300 × *g*, for 10 min at 4°C to remove cells, followed by a centrifugation at 2,000 × *g* for 20 min at 4°C to deplete cellular debris. Subsequently, samples were ultracentrifuged twice at 10,000 × *g* for 30 min at 4°C, the pellet was discarded, and the supernatant was submitted to an ultracentrifugation at 100,000 × *g*, for 2 h at 4°C to pellet sEVs. Finally, the pellet from the last step was washed with cold PBS, ultracentrifuged again at 100,000 × *g* for 2 h at 4°C, resuspended in 150 µL of cold PBS, and stored at −80°C. Ultracentrifugation steps were performed using a swinging bucket rotor SW 32 Ti in an Optima XPN 100K ultracentrifuge (Beckman Coulter, CA, USA) and 28.7-mL polyallomer conical tubes (Beckman Coulter).

sEV characterization: NTA

Size and concentration of sEVs were assessed through NTA using the NanoSight NS300 (Malvern Instruments, Malvern, UK). The system used an O-ring top plate and the sample was injected manually at an approximate flow of 1 mL every 20 s. sEVs were diluted in PBS until a concentration between 15 and 45 particles per frame was reached. For each sample, five videos of 30 s were recorded with the camera level set at 16. All the videos were processed with NTA 3.2 analytical software, using the software threshold between 2 and 4 depending on the quality of the videos.

sEV characterization: Protein quantification

sEV protein quantification was performed using the microBCA protein assay kit (Thermo Fisher Scientific, MA, USA), as per the manufacturer's instructions. Briefly, BSA was used to obtain a 10-point standard curve. Then, sEV samples were diluted 22 times in 2% (v/v) sodium dodecyl sulphate (SDS) to disrupt the sEV membrane and subsequently, 50 µL of the previous mix was pipetted, in duplicate, into a 96-well Corning Costar cell-culture plate (Corning, New York, USA). The reaction solution provided in the kit was added and incubated for 2 h at 37°C. Next, the plates were equilibrated at room temperature for 15 min and the absorbance at 562 nm was read in the microplate reader Synergy H1 (BioTek, VT, USA).

sEV characterization: TEM analyses

TEM analysis of sEVs was performed as previously described.[58] Briefly, samples were diluted 1:1 in 4% (v/v) PFA and placed on Formvar-carbon coated grids (TAAB Technologies) for 20 min at room temperature. After washing four times with PBS, grids were placed on a drop of 1% (v/v) glutaraldehyde for 5 min, followed by five washes with distilled water, 1 min each. In a dark environment, grids were

incubated with uranyl-oxalate solution, pH 7, for 5 min, and then placed on ice in contact with a solution of methyl cellulose (9:1) for 10 min. sEVs were imaged by a Tecnai G2 Spirit BioTWIN electron microscope (FEI Company) at 80 kV.

sEV characterization: Dynamic light scattering (DLS) analyses

Dynamic light scattering (DLS) measurements were done on a Zetasizer Nano ZS (Malvern). The sample was pre-equilibrated at 37°C for at least 60 s and each measurement was the average of 11 runs. Three consecutive measurements were performed for each sample to evaluate its stability. The results were analyzed by the equipment software considering the viscosity and refractive index of water at the measurement temperature and a refractive index of 1.59 for the scattering particles. The average size was taken from the analysis in volume distribution of particles.

sEV characterization: PALS

NanoBrook ZetaPALS Potential Analyzer (Brookhaven Instruments, Long Island, USA) was used for sEV surface charge measurement. Briefly, 5 μL of purified sEVs was diluted in 1500 μL of biological-grade ultrapure water (Fisher Scientific, NH, USA) and filtered twice through a 0.2-μm filter. sEVs were then placed in a disposable polystyrene cuvette and the electrode was immersed within the cuvette. Each sample was measured five times (using Smoluchowski module) at room temperature.

Modulation of sEVs with miR-425-5p or miR-scramble

Modulation of sEVs was accomplished using Exo-Fect according to the manufacturerś instructions. In brief, sEVs (29 μg of protein, equivalent to $\sim 6 \times 10^{10}$ particles) were incubated with Exo-Fect and 694 pmol miR-425-5p or miR-scramble for 10 min at 37°C. Assuming an 83% transfection efficiency,[19] the sEVs were modulated with a total of 576 pmol of miR-425-5p and miR-scramble, resulting in a total of 20 pmol of miR per 1 μg of sEVs. Modulated sEVs were aliquoted in individual tubes and stored at −80°C until further use.

Evaluation of miR-425-5p expression of modulated sEVs

To evaluate miR expression in sEVs upon modulation, total RNA was extracted using the RNeasy Micro Kit (#74004 Qiagen) as per the manufacturerś instructions. cDNA was synthesized for each sample from the amount of RNA extracted from 2^{10} sEVs using the Mir-X miR First-Strand Synthesis Kit (#638313, Takara) and and andqPCR was performed on the CFX Connect Real-Time System (Bio-Rad) using the NZYSpeedy qPCR Green Master Mix (2x) (#MB224, Nzytech). The universal 3′ mRQ primer (Takara) reverse primer was used and the forward primer sequence for miR-425-5p was: 5′-AAUG ACACGAUCACUCCCGUUGA-3′.

Labeling and loading of sEVs for uptake and intracellular trafficking analysis

sEVs were labeled with PKH67 (Sigma-Aldrich) according to the manufacture' instructions. Briefly, sEVs were diluted at 1:1 rate in the kit's buffer (diluent C) and PKH67 was diluted 1:5 (100 μL) in diluent C. The diluted sEVs and PKH67 were mixed and then incubated for 3 min at room temperature. Finally, the labeled sEVs were purified by ultracentrifugation at 100,000 × *g* for 2h at 4°C and the pellet containing labeled sEVs was resuspended in 100 μL of PBS. Afterward, the labeled sEVs were loaded with miR-425-5p as described above. Briefly, 10^{10} particles were mixed with 200 pmol of miR-425-5p in 10 μL of Exo-Fect (in a final volume of 150 μL) and incubated for 10 min at 37°C. To purify the sample, ExoQuick was added in a proportion of 1:5 (v/v) and incubated for 30 min at 4°C. Finally, the sEVs were centrifuged at 13,000 rpm for 3 min, the supernatant discarded and the pellet resuspended in 1× PBS to a final concentration of 1.5×10^9 part/mL loaded with 20 nM of miR-425-5p.

sEVs uptake assay

$CD34^+$-derived ECs (3×10^4 cells/well), fibroblasts (1.4×10^4 cells/well), and keratinocytes (6×10^4 cells/well) were seeded onto a 48-well plate and left to adhere overnight. Afterward, the cells were incubated with labeled native or miR-425-5p-modulated sEVs for 2, 4, and 24 h in EGM-2 Exo-depleted medium. To prepare Exo-depleted medium, EBM-2 (Lonza) medium supplemented with 2% (v/v) FBS was centrifuged at 100,000 × *g* for 18 h at 4°C and the supernatant was supplemented with the required growth factors and used for further experiments. At each time point, the cells were washed with PBS, detached with 0.1% (v/v) trypsin for 3 min, and centrifuged at 300 × *g* for 3 min at room temperature, followed by 5-min incubation with 0.4% (v/v) Trypan blue (Lonza). Lastly, the cells were centrifuged at 300 × *g* for 3 min at room temperature, resuspended in PBS and the fluorescence was quantified by flow cytometry (BD Accuri C6 Plus).

Intracellular trafficking of sEVs

$CD34^+$-derived ECs were seeded onto an Ibidi μ-slide angiogenesis plate at a density of 1×10^4 cells/well and left to adhere overnight. The following day, cells were incubated with PKH67-labeled sEVs (1.5×10^9 particles/mL) or PKH-labeled and miR-425-5p-modulated sEVs (1.5×10^9 particles/mL with 200 pmol of miR-425-5p) for 4 and 24 h in EGM-2 (Lonza) Exo-depleted medium. After incubation, cells were washed, incubated with 100 nM LysoTracker red DND-99 (Invitrogen) for 30 min at 37°C in cell-culture medium and fixed with 4% (v/v) PFA. Next, the cell membrane was stained with mouse anti-human CD31 (1:50, Dako) for 1 h at room temperature followed by incubation with Alexa $Fluor^{633}$ anti-mouse (1:1,000, Invitrogen) for 1 h at room temperature. Nuclei were stained with 1 μg/mL DAPI and the cells were analyzed using a Zeiss LSM 710 confocal scanning equipment with the excitation wavelengths of 405, 488 and 633 nm, and image acquisition was performed with Plan-Apochromat 40×/1.4 oil immersion objective. The images were analyzed with ImageJ software.

In vivo testing: Diabetic wound healing mouse model

All the experiments were performed in accordance with the European Community law for experimental animal studies (86/609/CEE and 2007/526/CE) and approved by the Institutional and Governmental Research Ethical Board. C57BL/6J mice (male, 8 weeks) purchased

from Charles River (Barcelona, Spain) were injected with 50 mg/kg of STZ (Sigma-Aldrich, Sintra, Portugal) in citrate buffer (0.1 M), intraperitoneally (i.p.), for five consecutive days to induce diabetes. Seven days after the STZ injection, blood glucose was measured using an Accu-Check Advantage glucometer (Roche, Amadora, Portugal), to confirm the diabetic state. Mice with blood glucose level above 250 mg/dL were considered diabetic. The animals were treated with 0.1–0.2 units of neutral protamine hagedorn (NPH) insulin, subcutaneously (s.c.), as needed, to avoid weight loss. The animals were kept diabetic for 6 weeks prior to the wound healing experiments. On the day of the experiment, mice were anesthetized with ketamine (100 mg/kg) and xylazine (10 mg/kg), i.p. After removing the hair from the back of the mice, two 6-mm full-thickness excisional wounds were biopsied and the wound area was traced every day onto acetate paper to follow the rate of wound closure up to 10 days post wounding. The wound size was determined with the ImageJ software (NIH) and results were presented as the percentage of original wound (day 0). In one case, immediately after wound induction, the wounds were treated with a complex of Lipofectamine RNAiMAX and 200 pmol miR-425-5p or miR-scramble in a final volume of 60 μL (four intradermal injections of 15 μL were applied at equidistant locations around the wound). PBS-treated wounds were used as a control. Additionally, sEVs were transfected with miR-425-5p or miR-scramble (see details above) and twice a day, 0.1 μg of sEVs transfected with 2 pmol miR-425-5p or miR-scramble were topically administered onto the wound (daily, 0.2 μg of sEVs and 4 pmol of miR-425-5p or miR-scramble). Animals were sacrificed after 10 days and samples immediately processed as described below. To study the mechanism of action of miR-425-5p *in vivo*, sEVs were transfected with miR-425-5p or miR-scramble using Exo-Fect (see details above) and, twice a day, 0.1 μg of sEVs transfected with 2 pmol of miR-425-5p or miR-scramble were topically administered onto the wound. Animals were sacrificed at day 2 and day 5 (after 2 days, 0.4 μg of sEVs and 8 pmol of miR-425-5p or miR-scramble; after 5 days, 1 μg of sEVs and 20 pmol of miR-425-5p or miR-scramble) and samples were immediately processed as described below.

In vivo testing: Immunohistochemical analysis

Following euthanasia at the selected time points, the wound tissue was excised together with the surrounding tissue and fixed in 10% (v/v) formalin (Sigma) for 24 h at 4°C. After 24 h, samples were embedded and frozen in blocks filled with cold optimal cutting temperature (OCT) compound and then cut into 9-μm-thick tissue sections. Sections were stained with anti-CD31 (ab28364; Abcam), keratin 14 (#905301; BioLegend), and keratin 5 (#905901; BioLegend) antibodies.

For CD31 staining, antigen retrieval was performed for 20 min using the citrate buffer at pH 6 at 97°C, blocked for 1 h with 5% (v/v) BSA, and then incubated overnight with rabbit anti-CD31 primary antibody (1:30) at 4°C. Samples were thoroughly washed with PBS and incubated for 1 h with the goat anti-rabbit Cy3 secondary antibody (Jackson ImmunoResearch; 1:300). Cell nuclei were counterstained DAPI (1 μg/mL). For quantification, CD31-stained vessels from five hotspots per wound were quantified and at least four wounds per experimental group were analyzed.

For keratin staining, sections were permeabilized for 10 min with 0.2% (v/v) Triton X, blocked for 1 h with 5% (v/v) BSA, and incubated overnight with rabbit anti-keratin 14 (1:1,000) and chicken anti-keratin 5 (1:200) primary antibodies at 4°C. Samples were thoroughly washed with PBS and incubated for 1 h with the secondary antibody goat anti-rabbit Cy3 (1:800) and goat anti-chicken Alexa^{488} (1:500). Cell nuclei were counterstained with DAPI (1 μg/mL). Images were analyzed using the InCell Bioanalyzer 2200 and, based on the keratin staining, the following parameters were assessed: wound edge (panniculus carnosus muscle gap), epithelial gap (distance between the epithelial tongues), re-epithelialization percentage (ratio of proliferative front over wound edge), and epidermal thickness (average thickness of the leading epithelial tongue from both ends).

SUPPLEMENTAL INFORMATION

Supplemental information can be found online at https://doi.org/10.1016/j.omtn.2022.03.018.

ACKNOWLEDGMENTS

This work was financed by the European Regional Development Fund (ERDF), through the Centro 2020 Regional Operational Program under project CENTRO-01-0145-FEDER-000014 and through the COMPETE2020 – Operational Program for Competitiveness and Internationalisation, Portuguese national funds via Fundação para a Ciência e a Tecnologia (FCT), under projects POCI-01-0145-FEDER-029919, UIDB/04539/2020, UIDP/04539/2020, and LA/P/0058/2020 and European project ERAatUC (reference 669088) and ResetAgeing (reference 952266). FCT supported H.F. (CEECIND/01880/2018), R.A. (SFRH/BD/129317/2017), M.B. (2020.09432.BD), S.A. (SFRH/BPD105172/20014), and E.L. (DL57/2016/CP1448/CT0024). The authors would like to acknowledge Daniel Johnston for proofreading the manuscript.

AUTHOR CONTRIBUTIONS

H.F., A.Z., R.A., S.A., M.B., I.A., M.L., A.B., C.S., T.B., E.L., A.d.J., H.A.B.P., and M.R.d.V. designed and conducted experiments and wrote the paper. J.T., L.G., P.d.C.M., P.H.A.Q., and L.F. designed experiments and wrote the paper.

DECLARATION OF INTERESTS

P.d.C.M. collaborates with Mirabilis Therapeutics. The other authors declare no competing interests.

REFERENCES

1. Rodrigues, M., Kosaric, N., Bonham, C.A., and Gurtner, G.C. (2019). Wound healing: a cellular perspective. Physiol. Rev. *99*, 665–706.

2. Ding, M.H., Lozoya, E.G., Rico, R.N., and Chew, S.A. (2020). The role of angiogenesis-inducing microRNAs in vascular tissue engineering. Tissue Eng. Part A *26*, 1283–1302.

3. Pasquinelli, A.E. (2012). MicroRNAs and their targets: recognition, regulation and an emerging reciprocal relationship. Nat. Rev. Genet. *13*, 271–282.
4. Small, E.M., and Olson, E.N. (2011). Pervasive roles of microRNAs in cardiovascular biology. Nature *469*, 336–342.
5. Welten, S.M., Bastiaansen, A.J., de Jong, R., de Vries, M.R., Peters, E.H., Boonstra, M., Sheikh, S.P., La Monica, N., Kandimalla, E.R., Quax, P.H., et al. (2014). Inhibition of 14q32 MicroRNAs miR-329, miR-487b, miR-494 and miR-495 increases neovascularization and blood flow recovery after ischemia. Circ. Res. *115*, 696–708.
6. Chan, Y.C., Roy, S., Khanna, S., and Sen, C.K. (2012). Downregulation of endothelial microRNA-200b supports cutaneous wound angiogenesis by desilencing GATA binding protein 2 and vascular endothelial growth factor receptor 2. Arterioscler. Thromb. Vasc. Biol. *32*, 1372–1382.
7. Lucas, T., Schafer, F., Muller, P., Eming, S.A., Heckel, A., and Dimmeler, S. (2017). Light-inducible antimiR-92a as a therapeutic strategy to promote skin repair in healing-impaired diabetic mice. Nat. Commun. *8*, 15162.
8. Bonauer, A., Carmona, G., Iwasaki, M., Mione, M., Koyanagi, M., Fischer, A., Burchfield, J., Fox, H., Doebele, C., Ohtani, K., et al. (2009). MicroRNA-92a controls angiogenesis and functional recovery of ischemic tissues in mice. Science *324*, 1710–1713.
9. Wang, J.-M., Tao, J., Chen, D.-D., Cai, J.-J., Irani, K., Wang, Q., Yuan, H., and Chen, A.F. (2014). MicroRNA miR-27b rescues bone marrow-derived angiogenic cell function and accelerates wound healing in type 2 diabetes mellitus. Arterioscler. Thromb. Vasc. Biol. *34*, 99–109.
10. Icli, B., Nabzdyk, C.S., Lujan-Hernandez, J., Cahill, M., Auster, M.E., Wara, A.K., Sun, X., Ozdemir, D., Giatsidis, G., Orgill, D.P., et al. (2016). Regulation of impaired angiogenesis in diabetic dermal wound healing by microRNA-26a. J. Mol. Cell Cardiol. *91*, 151–159.
11. Dallas, A., Trotsyuk, A., Ilves, H., Bonham, C.A., Rodrigues, M., Engel, K., Barrera, J.A., Kosaric, N., Stern-Buchbinder, Z.A., White, A., et al. (2019). Acceleration of diabetic wound healing with PHD2- and miR-210-targeting oligonucleotides. Tissue Eng. Part A *25*, 44–54.
12. Aday, S., Zoldan, J., Besnier, M., Carreto, L., Saif, J., Fernandes, R., Santos, T., Bernardino, L., Langer, R., Emanueli, C., et al. (2017). Synthetic microparticles conjugated with VEGF165 improve the survival of endothelial progenitor cells via microRNA-17 inhibition. Nat. Commun. *8*, 747.
13. Martello, A., Mellis, D., Meloni, M., Howarth, A., Ebner, D., Caporali, A., and Al Haj Zen, A. (2018). Phenotypic miRNA screen identifies miR-26b to promote the growth and survival of endothelial cells. Mol. Ther. Nucleic Acids *13*, 29–43.
14. Yin, H., Kanasty, R.L., Eltoukhy, A.A., Vegas, A.J., Dorkin, J.R., and Anderson, D.G. (2014). Non-viral vectors for gene-based therapy. Nat. Rev. Genet. *15*, 541–555.
15. Kalluri, R., and LeBleu, V.S. (2020). The biology, function, and biomedical applications of exosomes. Science *367*, eaau6977.
16. van Niel, G., D'Angelo, G., and Raposo, G. (2018). Shedding light on the cell biology of extracellular vesicles. Nat. Rev. Mol. Cell Biol. *19*, 213–228.
17. Yu, M., Liu, W., Li, J., Lu, J., Lu, H., Jia, W., and Liu, F. (2020). Exosomes derived from atorvastatin-pretreated MSC accelerate diabetic wound repair by enhancing angiogenesis via AKT/eNOS pathway. Stem Cell Res. Ther. *11*, 350.
18. Lv, Q., Deng, J., Chen, Y., Wang, Y., Liu, B., and Liu, J. (2020). Engineered human adipose stem-cell-derived exosomes loaded with miR-21-5p to promote diabetic cutaneous wound healing. Mol. Pharm. *17*, 1723–1733.
19. de Abreu, R.C., Ramos, C.V., Becher, C., Lino, M., Jesus, C., da Costa Martins, P.A., Martins, P.A.T., Moreno, M.J., Fernandes, H., and Ferreira, L. (2021). Exogenous loading of miRNAs into small extracellular vesicles. J. Extracell. Vesicles *10*, e12111.
20. Losordo, D.W., and Dimmeler, S. (2004). Therapeutic angiogenesis and vasculogenesis for ischemic disease - Part I: angiogenic cytokines. Circulation *109*, 2487–2491.
21. Kirkegaard, T., and Jaattela, M. (2009). Lysosomal involvement in cell death and cancer. Biochim. Biophys. Acta *1793*, 746–754.
22. Timmermans, F., Van Hauwermeiren, F., De Smedt, M., Raedt, R., Plasschaert, F., De Buyzere, M.L., Gillebert, T.C., Plum, J., and Vandekerckhove, B. (2007). Endothelial outgrowth cells are not derived from CD133+ cells or CD45+ hematopoietic precursors. Arterioscler. Thromb. Vasc. Biol. *27*, 1572–1579.
23. Pedroso, D.C., Tellechea, A., Moura, L., Fidalgo-Carvalho, I., Duarte, J., Carvalho, E., and Ferreira, L. (2011). Improved survival, vascular differentiation and wound healing potential of stem cells co-cultured with endothelial cells. PLoS One *6*, e16114.
24. Losordo, D.W., and Dimmeler, S. (2004). Therapeutic angiogenesis and vasculogenesis for ischemic disease - Part II: cell-based therapies. Circulation *109*, 2692–2697.
25. Catena, R., Muniz-Medina, V., Moralejo, B., Javierre, B., Best, C.J.M., Emmert-Buck, M.R., Greens, J.E., Baker, C.C., and Calvo, A. (2007). Increased expression of VEGF(121)/VEGF(165-189) ratio results in a significant enhancement of human prostate tumor angiogenesis. Int. J. Cancer *120*, 2096–2109.
26. Silva, E.A., Kim, E.S., Kong, H.J., and Mooney, D.J. (2008). Material-based deployment enhances efficacy of endothelial progenitor cells. Proc. Natl. Acad. Sci. U S A *105*, 14347–14352.
27. Song, M.S., Salmena, L., and Pandolfi, P.P. (2012). The functions and regulation of the PTEN tumour suppressor. Nat. Rev. Mol. Cell Biol. *13*, 283–296.
28. Rask-Madsen, C., and King, G.L. (2013). Vascular complications of diabetes: mechanisms of injury and protective factors. Cell Metabol. *17*, 20–33.
29. Beckman, J.A., and Creager, M.A. (2016). Vascular complications of diabetes. Circ. Res. *118*, 1771–1785.
30. Sheu, M.L., Ho, F.M., Yang, R.S., Chao, K.F., Lin, W.W., Lin-Shiau, S.Y., and Liu, S.H. (2005). High glucose induces human endothelial cell apoptosis through a phosphoinositide 3-kinase-regulated cyclooxygenase-2 pathway. Arterioscler. Thromb. Vasc. Biol. *25*, 539–545.
31. Veith, A.P., Henderson, K., Spencer, A., Sligar, A.D., and Baker, A.B. (2019). Therapeutic strategies for enhancing angiogenesis in wound healing. Adv. Drug Deliv. Rev. *146*, 97–125.
32. Henriques-Antunes, H., Cardoso, R.M.S., Zonari, A., Correia, J., Leal, E.C., Jimenez-Balsa, A., Lino, M.M., Barradas, A., Kostic, I., Gomes, C., et al. (2019). The kinetics of small extracellular vesicle delivery impacts skin tissue regeneration. ACS Nano *13*, 8694–8707.
33. Kamata, M., Liang, M., Liu, S., Nagaoka, Y., and Chen, I.S. (2010). Live cell monitoring of hiPSC generation and differentiation using differential expression of endogenous microRNAs. PLoS One *5*, e11834.
34. Maas, S.L., de Vrij, J., van der Vlist, E.J., Geragousian, B., van Bloois, L., Mastrobattista, E., Schiffelers, R.M., Wauben, M.H., Broekman, M.L., and Nolte-'t Hoen, E.N. (2015). Possibilities and limitations of current technologies for quantification of biological extracellular vesicles and synthetic mimics. J. Control. Release *200*, 87–96.
35. Gomez-Salinero, J.M., and Rafii, S. (2018). Endothelial cell adaptation in regeneration. Science *362*, 1116–1117.
36. Johnson, K.E., and Wilgus, T.A. (2014). Vascular endothelial growth factor and angiogenesis in the regulation of cutaneous wound repair. Adv. Wound Care (New Rochelle) *3*, 647–661.
37. Haniff, H.S., Knerr, L., Liu, X., Crynen, G., Bostrom, J., Abegg, D., Adibekian, A., Lekah, E., Wang, K.W., Cameron, M.D., et al. (2020). Design of a small molecule that stimulates vascular endothelial growth factor A enabled by screening RNA fold-small molecule interactions. Nat. Chem. *12*, 952–961.
38. Laflamme, M.A., Chen, K.Y., Naumova, A.V., Muskheli, V., Fugate, J.A., Dupras, S.K., Reinecke, H., Xu, C., Hassanipour, M., Police, S., et al. (2007). Cardiomyocytes derived from human embryonic stem cells in pro-survival factors enhance function of infarcted rat hearts. Nat. Biotechnol. *25*, 1015–1024.
39. Shang, L., Quan, A., Sun, H., Xu, Y., Sun, G., and Cao, P. (2019). MicroRNA-148a-3p promotes survival and migration of endothelial cells isolated from Apoe deficient mice through restricting circular RNA 0003575. Gene *711*, 143948.
40. Kaushik, K., and Das, A. (2020). TWIST1-Reprogrammed endothelial cell transplantation potentiates neovascularization-mediated diabetic wound tissue regeneration. Diabetes *69*, 1232–1247.
41. Duan, M., Zhang, Y., Zhang, H., Meng, Y., Qian, M., and Zhang, G. (2020). Epidermal stem cell-derived exosomes promote skin regeneration by downregulating transforming growth factor-beta1 in wound healing. Stem Cell Res. Ther. *11*, 452.
42. Raftrey, B., Williams, I.M., Rios Coronado, P.E., Fan, X., Chang, A.H., Zhao, M., Roth, R.K., Trimm, E., Racelis, R., D'Amato, G., et al. (2021). Dach1 extends artery networks and protects against cardiac injury. Circ. Res. *129*, 702–716.

43. Chang, A.H., Raftrey, B.C., D'Amato, G., Surya, V.N., Poduri, A., Chen, H.I., Goldstone, A.B., Woo, J., Fuller, G.G., Dunn, A.R., et al. (2017). DACH1 stimulates shear stress-guided endothelial cell migration and coronary artery growth through the CXCL12-CXCR4 signaling axis. Genes Dev. *31*, 1308–1324.

44. Li, Y., Yan, H., Guo, J., Han, Y., Zhang, C., Liu, X., Du, J., and Tian, X.-L. (2019). Down-regulated RGS5 by genetic variants impairs endothelial cell function and contributes to coronary artery disease. Cardiovasc. Res. *117*, 240–255.

45. Jin, Y., An, X., Ye, Z., Cully, B., Wu, J., and Li, J. (2009). RGS5, a hypoxia-inducible apoptotic stimulator in endothelial cells. J. Biol. Chem. *284*, 23436–23443.

46. Kobayashi, M., Wakabayashi, I., Suzuki, Y., Fujiwara, K., Nakayama, M., Watabe, T., and Sato, Y. (2021). Tubulin carboxypeptidase activity of vasohibin-1 inhibits angiogenesis by interfering with endocytosis and trafficking of pro-angiogenic factor receptors. Angiogenesis *24*, 159–176.

47. Takeda, E., Suzuki, Y., Yamada, T., Katagiri, H., and Sato, Y. (2017). Knockout of vasohibin-1 gene in mice results in healthy longevity with reduced expression of insulin receptor, insulin receptor substrate 1, and insulin receptor substrate 2 in their white adipose tissue. J. Aging Res. *2017*, 9851380.

48. Herrmann, I.K., Wood, M.J.A., and Fuhrmann, G. (2021). Extracellular vesicles as a next-generation drug delivery platform. Nat. Nanotechnol. *16*, 748–759.

49. de Abreu, R.C., Fernandes, H., da Costa Martins, P.A., Sahoo, S., Emanueli, C., and Ferreira, L. (2020). Native and bioengineered extracellular vesicles for cardiovascular therapeutics. Nat. Rev. Cardiol. *17*, 685–697.

50. Castano, C., Kalko, S., Novials, A., and Parrizas, M. (2018). Obesity-associated exosomal miRNAs modulate glucose and lipid metabolism in mice. Proc. Natl. Acad. Sci. U S A *115*, 12158–12163.

51. Zeng, Z., Li, Y., Pan, Y., Lan, X., Song, F., Sun, J., Zhou, K., Liu, X., Ren, X., Wang, F., et al. (2018). Cancer-derived exosomal miR-25-3p promotes pre-metastatic niche formation by inducing vascular permeability and angiogenesis. Nat. Commun. *9*, 5395.

52. Morton, M.C., Neckles, V.N., Seluzicki, C.M., Holmberg, J.C., and Feliciano, D.M. (2018). Neonatal subventricular zone neural stem cells release extracellular vesicles that act as a microglial morphogen. Cell Rep. *23*, 78–89.

53. Xiao, Y., Reis, L.A., Feric, N., Knee, E.J., Gu, J., Cao, S., Laschinger, C., Londono, C., Antolovich, J., McGuigan, A.P., et al. (2016). Diabetic wound regeneration using peptide-modified hydrogels to target re-epithelialization. Proc. Natl. Acad. Sci. U S A *113*, E5792–E5801.

54. Zhu, Y., Cankova, Z., Iwanaszko, M., Lichtor, S., Mrksich, M., and Ameer, G.A. (2018). Potent laminin-inspired antioxidant regenerative dressing accelerates wound healing in diabetes. Proc. Natl. Acad. Sci. U S A *115*, 6816–6821.

55. Griffin, D.R., Weaver, W.M., Scumpia, P.O., Di Carlo, D., and Segura, T. (2015). Accelerated wound healing by injectable microporous gel scaffolds assembled from annealed building blocks. Nat. Mater. *14*, 737–744.

56. Livak, K.J., and Schmittgen, T.D. (2001). Analysis of relative gene expression data using real-time quantitative PCR and the 2(-Delta Delta C(T)) Method. Methods *25*, 402–408.

57. van dey Kwast, R.V.C.T., van Ingen, E., Parma, L., Peters, H.A.B., Quax, P.H.A., and Nossent, A.Y. (2018). Adenosine-to-Inosine editing of MicroRNA-487b alters target gene selection after ischemia and promotes neovascularization. Circ. Res. *122*, 444–456.

58. Thery, C., Amigorena, S., Raposo, G., and Clayton, A. (2006). Isolation and characterization of exosomes from cell culture supernatants and biological fluids. Curr. Protoc. Cell Biol. *Chapter 3*, 3–22.